

Soft gluon resummation for associated squark-electroweakino production at the LHC

Juri Fiaschi^a, Benjamin Fuks^b, Michael Klasen^c and Alexander Neuwirth^c

^a*Department of Mathematical Sciences, University of Liverpool, Liverpool L69 3BX, United Kingdom*

^b*Laboratoire de Physique Théorique et Hautes Énergies (LPTHE), UMR 7589, Sorbonne Université et CNRS, 4 place Jussieu, 75252 Paris Cedex 05, France*

^c*Institut für Theoretische Physik, Westfälische Wilhelms-Universität Münster, Wilhelm-Klemm-Straße 9, 48149 Münster, Germany*

E-mail: fiaschi@liverpool.ac.uk, fuks@lpthe.jussieu.fr,
michael.klasen@uni-muenster.de, alexander.neuwirth@uni-muenster.de

ABSTRACT: We perform a threshold resummation calculation for the associated production of squarks and electroweakinos at the LHC to the next-to-leading logarithmic (NLL) accuracy. Analytical results for the process-dependent soft anomalous dimension and the hard matching coefficient are presented. The resummed results are matched to fixed-order predictions at next-to-leading order (NLO) in QCD, which are generalised to scenarios with non-universal squark masses and mixings. Numerically, the NLL contributions increase the total NLO cross section by 2% to 6% for squark masses ranging from 1 TeV to 3 TeV, respectively, and they reduce the dependence of the predictions on the factorisation and renormalisation scales from typically $\pm 10\%$ to below $\pm 5\%$. Our NLO and NLO+NLL calculations have been implemented in the publicly available program RESUMMINO.

KEYWORDS: Perturbative QCD, resummation, supersymmetry, hadron colliders

Contents

1	Introduction	1
2	Soft gluon resummation	3
2.1	Production of squarks and electroweakinos at leading and next-to-leading order	3
2.2	Refactorisation	5
2.3	Hard matching coefficient	7
2.4	Matching and expansion	8
3	Numerical Results	9
3.1	Validation of our NLO implementation	9
3.2	Invariant mass distributions	11
3.3	Total cross sections and their scale uncertainty	13
3.4	Parton density uncertainties of the total cross section	14
3.5	Squark and gaugino mass dependence of the total cross section	16
4	Conclusion	16
A	Soft anomalous dimension	18
B	Lists of total cross sections	20

1 Introduction

In the search for physics beyond the Standard Model (SM), supersymmetry (SUSY) offers a very promising avenue. By relating bosons and fermions, it stabilises the Higgs boson mass with respect to quantum corrections, allows for the unification of the gauge couplings and provides a dark matter candidate, thus solving several long-standing problems of the SM simultaneously. Within the Minimal Supersymmetric Standard Model (MSSM) [1, 2], each degree of freedom of the SM is associated with a superpartner, that differs only by half a unit in spin. The scalar partners of the left- and right-handed quarks mix, as do the higgsino, bino and wino interaction eigenstates, which after electroweak symmetry breaking form neutral and charged so-called electroweakinos (neutralinos and charginos). Since these particles have not yet been discovered, it must be assumed that supersymmetry is broken, which increases the masses of the supersymmetric particles with respect to those of their SM partners. With the assumption of conserved R -parity, a neutral lightest supersymmetric particle (LSP) then has all the right properties to be one of the most promising dark matter candidates, *i.e.* a weakly interacting massive particle (WIMP).

Both the upcoming Run 3 of the Large Hadron Collider (LHC) and its planned extension to high luminosity (HL-LHC) will provide access to very massive new particles [3–5]. In

supersymmetry, the generally dominant production processes are those involving the strong interaction and thus concern the pair production of squarks and gluinos. As a consequence of the current and expected bounds on these states, they might be too massive to be pair-produced at the LHC. This restriction can be lifted by considering the single production of a squark or a gluino in association with a (typically lighter) electroweakino. These processes then also have the advantage of providing insights not only on the supersymmetric masses, but also on the supersymmetric interactions [6–8].

Only precise theoretical predictions allow for a reliable comparison between theory and experiment. Already by going from leading order (LO) to next-to-leading order (NLO) in perturbative QCD, the theoretical uncertainty originating from the arbitrary choice of factorisation and renormalisation scales is reduced. However, with the possibility of light SUSY particles being excluded by direct searches at the LHC, the current mass limits imply that in any SUSY production process the kinematic configuration approaches the production threshold. This results in large threshold logarithms ruining the convergence of the perturbative series, so that they must be resummed. This resummation procedure has been known for quite some time at the leading logarithmic (LL) and next-to-leading-logarithmic (NLL) accuracy and in some cases beyond and has been found to generally further reduce the theoretical uncertainty inherent in the perturbative calculation [9–13].

In the last decade the precise investigation of slepton pair [14–20], electroweakino pair [21–28] and electroweakino-gluino [29] production beyond NLO was accomplished. Similarly, improved predictions in the strong sector exist for squark and gluino pair production [30–36]. In this work we focus on the production of a squark and an electroweakino at hadron colliders. Since this process involves both weak [$\mathcal{O}(\alpha_{\text{EM}})$] and strong [$\mathcal{O}(\alpha_s)$] interactions at leading order, the resulting cross section is of intermediate size. The simplest process in this category involves the production of a first- or second-generation squark together with a lightest neutralino. This process manifests itself through a hard jet originating from the squark decay and missing transverse energy from the two neutralinos leaving the detector invisibly, one of them being a decay product of the squark and the other one being directly produced in the hard process. Such a monojet signal is particularly well-studied in the context of dark matter production at colliders [37, 38]. In recent analyses by the CMS collaboration, squark masses below 1.6 TeV were excluded in four mass-degenerate squark flavour models, assuming production with a light neutralino $\tilde{\chi}_1^0$. This limit is reduced to 1.1 TeV for a single kinematically reachable squark [39–41]. Similarly, the ATLAS collaboration gives limits of 1.4 TeV and 1.0 TeV [42, 43].

In this paper, we present a threshold resummation calculation for the associated production of squarks and electroweakinos at the NLO+NLL accuracy. The structure of this work is as follows: In section 2, we compute the production cross section at leading and next-to-leading order and give a brief summary of the ingredients required for threshold resummation. The numerical validation of our NLO calculation and our new results up to NLO+NLL accuracy are given in section 3 for various benchmark scenarios. We summarise our work and conclude in section 4.

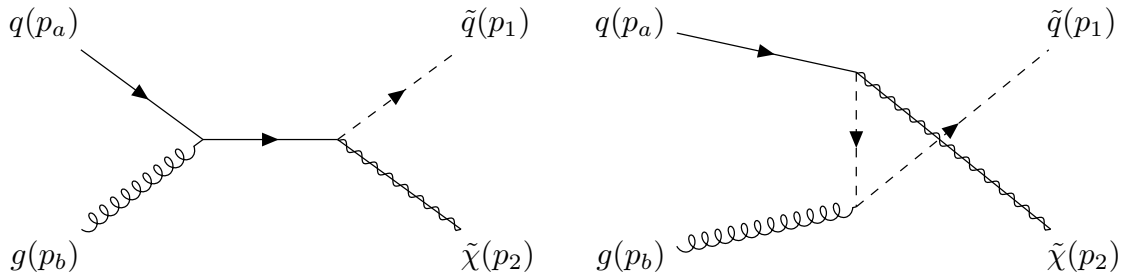


Figure 1: Tree-level s - (left) and u -channel (right) Feynman diagrams for the associated production of a squark and an electroweakino at hadron colliders.

2 Soft gluon resummation

We begin this work with a derivation of LO and NLO expressions for the associated production of a squark and an electroweakino at hadron colliders in section 2.1. Then, section 2.2 explains refactorisation and resummation up to NLL accuracy and includes a computation of the soft anomalous dimension associated with the process considered. In section 2.3 we present the NLO hard matching coefficient, which is then used together with the soft anomalous dimension in section 2.4 to consistently combine fixed-order and resummed predictions at the NLO+NLL accuracy.

2.1 Production of squarks and electroweakinos at leading and next-to-leading order

To calculate the total hadronic cross section σ_{AB} for the process considered, we convolute the partonic cross section $d\sigma_{ab}$ with factorisation-scale dependent parton distribution functions (PDFs) $f_{i/h}(x_i, \mu_F^2)$ for a particle i of momentum fraction x_i in a hadron h ,

$$\sigma_{AB} = \int M^2 \frac{d\sigma_{AB}}{dM^2}(\tau) = \sum_{a,b} \int_0^1 dx_a dx_b dz \left[x_a f_{a/A}(x_a, \mu_F^2) \right] \left[x_b f_{b/B}(x_b, \mu_F^2) \right] \times \left[z d\sigma_{ab}(z, M^2, \mu_R^2, \mu_F^2) \right] \delta(\tau - x_a x_b z), \quad (2.1)$$

where $\tau = M^2/S$ is the ratio of the squared invariant mass M^2 over the hadronic centre-of-mass energy S [44].

The partonic fraction $z = \tau/(x_a x_b) = M^2/s$ is defined by the ratio of the squared invariant mass to the partonic centre-of-mass energy $s = x_a x_b S$ and equals one at leading order. The partonic cross section

$$\sigma_{ab}(s) = \int_2 d\sigma_{ab} = \int \frac{1}{2s} \overline{|\mathcal{M}|^2} d\text{PS}^{(2)} \quad (2.2)$$

is related to the squared and averaged matrix element $\overline{|\mathcal{M}|^2}$ by the usual flux factor $1/(2s)$ and the integration over the two-particle phase space $d\text{PS}^{(2)}$.

The associated production of a squark and an electroweakino with masses $m_{\tilde{q}}$ and $m_{\tilde{\chi}}$ occurs at a hadron collider at LO through the annihilation of a (massless) quark and a

gluon. Charge conservation restricts the possible partonic processes to

$$q_{u,d}(p_a) g(p_b) \rightarrow \tilde{q}_{u,d}(p_1) \tilde{\chi}_k^0(p_2) \quad \text{and} \quad q_{u,d}(p_a) g(p_b) \rightarrow \tilde{q}_{d,u}(p_1) \tilde{\chi}_k^\pm(p_2), \quad (2.3)$$

where k identifies the neutralino ($\tilde{\chi}_k^0$, $k = 1, \dots, 4$) or chargino ($\tilde{\chi}_k^\pm$, $k = 1, 2$) mass eigenstate and $p_{a,b}$ and $p_{1,2}$ refer to the four-momenta of the initial- and final-state particles, respectively. The corresponding Born diagrams are shown in fig. 1. The squared matrix elements associated with the s -channel quark exchange diagram (left), the u -channel squark exchange diagram (right) and their interference can be expressed as functions of the usual Mandelstam variables $s = (p_a + p_b)^2$, $t = (p_a - p_1)^2$ and $u = (p_a - p_2)^2$, *i.e.* as

$$|\mathcal{M}_s|^2 = \frac{g_s^2 C_A C_F B}{s} 2(m_{\tilde{\chi}}^2 - t), \quad (2.4)$$

$$|\mathcal{M}_u|^2 = -\frac{g_s^2 C_A C_F B}{(u - m_{\tilde{q}}^2)^2} 2(m_{\tilde{\chi}}^2 - u)(m_{\tilde{q}}^2 + u) \quad \text{and} \quad (2.5)$$

$$2 \text{Re}[\mathcal{M}_s \mathcal{M}_u^\dagger] = 2 \frac{g_s^2 C_A C_F B}{s(u - m_{\tilde{q}}^2)} \left(2(m_{\tilde{\chi}}^4 - m_{\tilde{q}}^4) + m_{\tilde{q}}^2(2u - 3s) - 2m_{\tilde{\chi}}^2(2m_{\tilde{q}}^2 + u) - su \right). \quad (2.6)$$

They are all proportional to the squared electroweakino-squark-quark coupling

$$B \equiv R_{Ijk} L'_{Ijk} + L_{Ijk} R'_{Ijk} = R_{Ijk} R_{Ijk}^* + L_{Ijk} L_{Ijk}^* = |R_{Ijk}|^2 + |L_{Ijk}|^2, \quad (2.7)$$

where the capitalised index I labels the quark generation, the lower-case index j refers to the squark eigenstate and the index k is related as above to the electroweakino eigenstate. The definitions of the various left- and right-handed couplings $L^{(\prime)}$ and $R^{(\prime)}$ are provided in Refs. [2, 29, 45]. Using arbitrary squark mixings and mass eigenstates opens the possibility to study SUSY flavour violation [46–51]. The total spin- and colour-averaged squared amplitude then reads

$$\overline{|\mathcal{M}|^2} = \frac{1}{96} \left(|\mathcal{M}_s|^2 + |\mathcal{M}_u|^2 + 2 \text{Re}[\mathcal{M}_s \mathcal{M}_u^\dagger] \right). \quad (2.8)$$

The NLO corrections to this cross section are well-known [6–8]. They involve one-loop self-energy, vertex and box corrections interfering with tree-level diagrams, as well as squared real gluon and quark emission diagrams, from which intermediate on-shell squark and gluino resonant contributions have to be subtracted to avoid spoiling the convergence of the perturbative series [52, 53]. We have calculated the full NLO cross section using dimensional regularisation of ultraviolet (UV) and infrared (IR) divergences, on-shell renormalisation for all squark and gluino masses and wave functions, and $\overline{\text{MS}}$ renormalisation for the couplings with the exception of the strong coupling g_s . The latter is renormalised by subtracting, at zero-momentum transfer, all massive particle contributions and $\overline{\text{MS}}$ contributions of all massless particles from the gluon self-energy [54–56]. In order to avoid the violation of SUSY invariance by the introduction of a mismatch between the strong coupling g_s and the quark-squark-gluino Yukawa coupling \hat{g}_s at one loop, we shift \hat{g}_s by a finite contribution, allowing us to restore SUSY and to make use of the above-mentioned renormalisation scheme [57].

Real and virtual contributions are combined with the help of the dipole subtraction method to cancel infrared and collinear divergences [58–60]. This method splits the pure NLO cross section into separately finite virtual and real contributions and a collinear counterterm consisting of two insertion operators \mathbf{P} and \mathbf{K} ,

$$\begin{aligned} \sigma^{\text{NLO}} = & \int_3 \left[d\sigma^{\text{R}} - d\sigma^{\text{A}} \right]_{\epsilon=0} + \int_2 \left[d\sigma^{\text{V}} + \int_1 d\sigma^{\text{A}} \right]_{\epsilon=0} \\ & + \int_0^1 dx \int_2 \left[d\sigma^{\text{B}}(xp) \otimes (\mathbf{P} + \mathbf{K})(x) \right]_{\epsilon=0}. \end{aligned} \quad (2.9)$$

In this expression the integration domain denotes the number of final-state particles. Moreover, the auxiliary cross section σ^{A} shifts the infrared divergences such that the integrations over both the two- and three-particle phase spaces are numerically possible without changing the total result.

2.2 Refactorisation

After the cancellation of soft and collinear divergences among the real and virtual corrections, large logarithms remain near threshold [61, 62]. They arise between the constrained integration over the real emission phase space and the integration of virtual loops and take the form

$$\left(\frac{\alpha_s}{2\pi} \right)^n \left[\frac{\log^m(1-z)}{1-z} \right]_+, \quad (2.10)$$

with $m \leq 2n - 1$. The variable $1 - z = 1 - M^2/s$ describes the energy fraction of an additional emitted gluon or massless quark and thus quantifies the distance to the partonic threshold. For soft emitted particles ($z \rightarrow 1$), truncating the perturbative calculation at a fixed order does not give a reliable prediction, so that the logarithms must be resummed to all orders in α_s .

To calculate soft gluon emission up to all orders, kinematic and dynamical factorisation are necessary. Kinematic factorisation is possible by transforming the constituents of eq. (2.1) into Mellin space

$$F(N) = \int_0^1 dy y^{N-1} F(y), \quad (2.11)$$

with $F = \sigma_{AB}, \sigma_{ab}, f_{a/A}, f_{b/B}$ and $y = \tau, z, x_a, x_b$, respectively. We obtain

$$M^2 \frac{d\sigma_{AB}}{dM^2}(N-1) = \sum_{a,b} f_{a/A}(N, \mu_F^2) f_{b/B}(N, \mu_F^2) \sigma_{ab}(N, M^2, \mu_F^2, \mu_R^2), \quad (2.12)$$

such that the phase space factorises. In this expression, the large logarithms now depend on the Mellin variable N . Dynamical factorisation can then be achieved by relying on eikonal Feynman rules. The partonic cross section can be refactorised and resummed to

$$\begin{aligned} \sigma_{ab \rightarrow ij}(N, M^2, \mu_F^2, \mu_R^2) = & \sum_I \mathcal{H}_{ab \rightarrow ij, I}(M^2, \mu_F^2, \mu_R^2) \Delta_a(N, M^2, \mu_F^2, \mu_R^2) \\ & \times \Delta_b(N, M^2, \mu_F^2, \mu_R^2) \Delta_{ab \rightarrow ij, I}(N, M^2, \mu_F^2, \mu_R^2), \end{aligned} \quad (2.13)$$

in which the hard function is given by

$$\mathcal{H}_{ab \rightarrow ij, I}(M^2, \mu_F^2, \mu_R^2) = \sum_{n=0}^{\infty} \left(\frac{\alpha_s}{2\pi} \right)^n \mathcal{H}_{ab \rightarrow ij, I}^{(n)}(M^2, \mu_F^2, \mu_R^2). \quad (2.14)$$

This quantity is further discussed in section 2.3 [12, 13, 44]. The irreducible colour representation index I is dropped from now on, since squark-electroweakino associated production involves only a single colour tensor. The soft wide-angle function $\Delta_{ab \rightarrow ij}$ and the soft collinear radiation functions $\Delta_{a,b}$ exponentiate [63],

$$\Delta_a \Delta_b \Delta_{ab \rightarrow ij} = \exp \left[LG_{ab}^{(1)}(\lambda) + G_{ab \rightarrow ij}^{(2)}(\lambda, M^2, \mu_F^2, \mu_R^2) + \dots \right], \quad (2.15)$$

with $\lambda = \alpha_s \beta_0 L / (2\pi)$, $L = \log \bar{N}$ and $\bar{N} = N e^{\gamma_E}$. The above expression contains the leading-logarithmic $G_{ab}^{(1)}$ and next-to-leading logarithmic $G_{ab \rightarrow ij}^{(2)}$ contributions [10, 11]. They are given by

$$G_{ab}^{(1)}(\lambda) = g_a^{(1)}(\lambda) + g_b^{(1)}(\lambda), \quad (2.16)$$

$$G_{ab \rightarrow ij}^{(2)}(\lambda, M^2, \mu_F^2, \mu_R^2) = g_a^{(2)}(\lambda, M^2, \mu_F^2, \mu_R^2) + g_b^{(2)}(\lambda, M^2, \mu_F^2, \mu_R^2) + h_{ab \rightarrow ij}^{(2)}(\lambda), \quad (2.17)$$

with

$$g_a^{(1)} = \frac{A_a^{(1)}}{2\beta_0 \lambda} [2\lambda + (1 - 2\lambda) \log(1 - 2\lambda)], \quad (2.18)$$

$$\begin{aligned} g_a^{(2)} &= \frac{A_a^{(1)} \beta_1}{2\beta_0^3} \left[2\lambda + \log(1 - 2\lambda) + \frac{1}{2} \log^2(1 - 2\lambda) \right] - \frac{A_a^{(2)}}{2\beta_0^2} [2\lambda + \log(1 - 2\lambda)] \\ &+ \frac{A_a^{(1)}}{2\beta_0} \left[\log(1 - 2\lambda) \log \left(\frac{M^2}{\mu_R^2} \right) + 2\lambda \log \left(\frac{\mu_F^2}{\mu_R^2} \right) \right]. \end{aligned} \quad (2.19)$$

The resummation coefficients entering those quantities are

$$A_a^{(1)} = 2C_a \quad \text{and} \quad A_a^{(2)} = 2C_a \left[\left(\frac{67}{18} - \frac{\pi^2}{6} \right) C_A - \frac{5}{9} n_f \right], \quad (2.20)$$

with $C_a = C_F$ for quarks and $C_a = C_A$ for gluons. The last term in eq. (2.17) consists of the process-dependent contributions related to large-angle soft-gluon emissions. It reads

$$h_{ab \rightarrow ij}^{(2)}(\lambda) = \frac{\log(1 - 2\lambda)}{2\beta_0} D_{ab \rightarrow ij}^{(1)} = \frac{\log(1 - 2\lambda)}{2\beta_0} \frac{2\pi}{\alpha_s} \text{Re}(\bar{\Gamma}_{ab \rightarrow ij}). \quad (2.21)$$

The one-loop coefficient $D_{ab \rightarrow ij}^{(1)}$ does not vanish for squark-gaugino production, since soft gluons can be radiated off the final-state squark, and it depends on the modified soft anomalous dimension

$$\bar{\Gamma}_{qg \rightarrow \tilde{q}\tilde{\chi}} = \frac{\alpha_s}{2\pi} \left\{ C_F \left[2 \log \left(\frac{m_{\tilde{q}}^2 - t}{\sqrt{s} m_{\tilde{q}}} \right) - 1 + i\pi \right] + C_A \log \left(\frac{m_{\tilde{q}}^2 - u}{m_{\tilde{q}}^2 - t} \right) \right\}, \quad (2.22)$$

that has been derived in appendix A.

2.3 Hard matching coefficient

The resummation of the logarithmic contributions as performed in eq. (2.15) scales with the hard function $\mathcal{H}_{ab \rightarrow ij}(M^2, \mu_F^2, \mu_R^2)$, as shown in eq. (2.13). Including higher-order contribution in the hard function hence further improves the accuracy of the predictions. Therefore, in addition to the LO term

$$\mathcal{H}_{ab \rightarrow ij}^{(0)}(M^2, \mu_F^2, \mu_R^2) = \sigma_{ab \rightarrow ij}^{(0)}(M^2), \quad (2.23)$$

we include the N -independent parts of the NLO cross section in the one-loop hard matching coefficient,

$$\mathcal{H}_{ab \rightarrow ij}^{(1)}(M^2, \mu_F^2, \mu_R^2) = \sigma_{ab \rightarrow ij}^{(0)}(M^2) C_{ab \rightarrow ij}^{(1)}(M^2, \mu_F^2, \mu_R^2). \quad (2.24)$$

To compute this coefficient, we begin with the full NLO cross section of eq. (2.9). We first neglect the real emission contributions due to the three-particle phase space suppression close to threshold [31, 34]. The virtual contributions $d\sigma^V$ and the integrated dipoles $\int_1 d\sigma^A$ in eq. (2.9) correspond to a contribution proportional to $\delta(1-z)$, that is thus constant in N after a Mellin transform. The collinear remainder is split into two pieces related to the insertion operators \mathbf{P} and \mathbf{K} , in which only the former depends on the factorisation scale μ_F [58–60]. After discarding any $\mathcal{O}(1/N)$ contribution that vanishes in the large- N limit, only the diagonal terms survive. We obtain for the initial quark

$$\begin{aligned} \langle \mathbf{P}(N) \rangle_q &= \frac{\alpha_s}{2\pi} \left(\log \bar{N} - \frac{3}{4} \right) \left(2C_F \log \frac{\mu_F^2}{m_{\bar{q}}^2 - t} - C_A \log \frac{s}{m_{\bar{q}}^2 - t} \right), \\ \langle \mathbf{K}(N) \rangle_q &= \frac{\alpha_s}{2\pi} \left\{ C_F \left(2 \log^2 \bar{N} + \frac{\pi^2}{2} - \frac{\gamma_q}{C_F} - \frac{K_q}{C_F} \right) \right. \\ &\quad \left. + \left(C_F - \frac{C_A}{2} \right) \left[2 \log \bar{N} \left(1 + \log \frac{m_{\bar{q}}^2}{m_{\bar{q}}^2 - t} \right) + \mathcal{Q} \right] \right\}, \end{aligned} \quad (2.25)$$

with

$$\begin{aligned} \mathcal{Q} &= \frac{m_{\bar{q}}^2 - t}{2m_{\bar{q}}^2 - t} + \frac{3m_{\bar{q}}}{m_{\bar{q}} + \sqrt{2m_{\bar{q}}^2 - t}} + \log \frac{m_{\bar{q}}^2}{2m_{\bar{q}}^2 - t} \left(1 + 2 \log \frac{m_{\bar{q}}^2}{m_{\bar{q}}^2 - t} \right) \\ &\quad - \frac{3}{2} \log \frac{3m_{\bar{q}}^2 - t - 2m_{\bar{q}} \sqrt{2m_{\bar{q}}^2 - t}}{m_{\bar{q}}^2 - t} + 2\text{Li}_2 \left(\frac{2m_{\bar{q}}^2 - t}{m_{\bar{q}}^2} \right) - \frac{\gamma_{\bar{q}}}{C_F}. \end{aligned} \quad (2.26)$$

For the initial gluon, we find

$$\begin{aligned} \langle \mathbf{P}(N) \rangle_g &= \frac{\alpha_s}{2\pi} \left(C_A \log \bar{N} - \frac{\beta_0}{2} \right) \log \frac{\mu_F^4}{s(m_{\bar{q}}^2 - u)}, \\ \langle \mathbf{K}(N) \rangle_g &= \frac{\alpha_s}{2\pi} \frac{C_A}{2} \left[4 \log^2 \bar{N} + 2 \log \bar{N} \left(1 + \log \frac{m_{\bar{q}}^2}{m_{\bar{q}}^2 - u} \right) + \pi^2 - \frac{2\gamma_g}{C_A} - \frac{2K_g}{C_A} + \mathcal{G} \right], \end{aligned} \quad (2.27)$$

with

$$\begin{aligned} \mathcal{G} = & \frac{m_{\bar{q}}^2 - u}{2m_{\bar{q}}^2 - u} + \log \frac{m_{\bar{q}}^2}{2m_{\bar{q}}^2 - u} \left(1 + 2 \log \frac{m_{\bar{q}}^2}{m_{\bar{q}}^2 - u} \right) + 2\text{Li}_2 \left(\frac{2m_{\bar{q}}^2 - u}{m_{\bar{q}}^2} \right) - \frac{\gamma_{\bar{q}}}{C_F} \\ & + \frac{\beta_0}{C_A} \left(\log \frac{3m_{\bar{q}}^2 - u - 2m_{\bar{q}}\sqrt{2m_{\bar{q}}^2 - u}}{m_{\bar{q}}^2 - u} + \frac{2m_{\bar{q}}}{\sqrt{2m_{\bar{q}}^2 - u} + m_{\bar{q}}} \right). \end{aligned} \quad (2.28)$$

In all these expressions, the two-body phase space Mandelstam variables are defined according to the particle ordering of eq. (2.3), and the various constants are [59]

$$\begin{aligned} \gamma_q &= \frac{3}{2}C_F, & K_q &= \left(\frac{7}{2} - \frac{\pi^2}{6} \right) C_F, \\ \gamma_g &= \beta_0 = \frac{11}{6}C_A - \frac{2}{3}T_R N_f, & K_g &= \left(\frac{67}{18} - \frac{\pi^2}{6} \right) C_A - \frac{10}{9}T_R N_f, \\ \gamma_{\bar{q}} &= 2C_F, & K_{\bar{q}} &= \left(4 - \frac{\pi^2}{6} \right) C_F. \end{aligned} \quad (2.29)$$

As we have ignored any $1/N$ terms in the above computation of the hard matching coefficient, we employ the standard collinear unimproved resummation formalism as opposed to the collinear improved one of Refs. [64–67]. While only the N -independent terms are necessary in practice, we included the logarithmic terms in the above expressions to be able to validate analytically the re-expansion of the resummed cross section at $\mathcal{O}(\alpha_s^2)$ in section 2.4.

2.4 Matching and expansion

So far we have computed a fixed order cross section σ^{NLO} and a resummed cross section $\sigma^{\text{Res.}}$. As the latter is a good approximation near threshold and the former far from it, they should be consistently combined. Therefore, we sum up both contributions and remove the terms that are accounted for both in the resummed and the fixed-order predictions, thus avoiding any double counting. A consistent matching is achieved by re-expanding $\sigma^{\text{Res.}}$ at $\mathcal{O}(\alpha_s^2)$ and subtracting this quantity $\sigma^{\text{Exp.}}$ from the sum of the resummed and fixed-order results,

$$\sigma_{ab} = \sigma_{ab}^{\text{NLO}} + \sigma_{ab}^{\text{Res.}} - \sigma_{ab}^{\text{Exp.}}. \quad (2.30)$$

The expansion is given in terms of the first- ($\mathcal{H}^{(0)}$) and second-order ($\mathcal{H}^{(1)}$) hard function coefficients of section 2.3,

$$\begin{aligned} \sigma_{ab}^{\text{Exp.}} = & \mathcal{H}_{ab \rightarrow ij}^{(0)}(M^2, \mu^2) + \frac{\alpha_s}{2\pi} \mathcal{H}_{ab \rightarrow ij}^{(1)}(M^2, \mu^2) + \frac{\alpha_s}{2\pi} \mathcal{H}_{ab \rightarrow ij}^{(0)}(M^2, \mu^2) \\ & \times \left(\left(A_a^{(1)} + A_b^{(1)} \right) \left(\log \bar{N} + \log \frac{\mu_F^2}{s} \right) - 2D_{ab \rightarrow ij}^{(1)} \right) \log \bar{N}. \end{aligned} \quad (2.31)$$

We can verify that the leading logarithmic terms in $\log^2 \bar{N}$ agree with those of the \mathbf{K} -operators for quarks ($A_q^{(1)} = 2C_F$) and gluons ($A_g^{(1)} = 2C_A$) in eq. (2.25) and eq. (2.27). Moreover, combining the next-to-leading logarithmic terms in $\log \bar{N}$ originating from the

soft anomalous dimension in eq. (2.22) and the terms in $\log(\mu_F^2/s)$ from eq. (2.31), we recover the same terms as in the sum of the contributions of the \mathbf{P} and \mathbf{K} operators for quarks and gluons taken separately,

$$2C_F \left[\log \frac{\mu_F^2}{m_{\tilde{q}}^2 - t} + \log \frac{m_{\tilde{q}}^2}{m_{\tilde{q}}^2 - t} + 1 \right] + (u \leftrightarrow t), \quad (2.32)$$

$$2C_A \left[\log \frac{\mu_F^2}{s} + \log \frac{m_{\tilde{q}}^2 - t}{m_{\tilde{q}}^2 - u} \right] + (u \leftrightarrow t). \quad (2.33)$$

The partonic cross section in Mellin space must finally be multiplied with the N -moments of the PDFs, and an inverse Mellin transformation must be applied [68, 69],

$$M^2 \frac{d\sigma_{AB}}{dM^2}(\tau) = \frac{1}{2\pi i} \int dN \tau^{-N} M^2 \frac{d\sigma_{AB}}{dM^2}(N). \quad (2.34)$$

Details can be found in Ref. [29].

3 Numerical Results

For our numerical predictions, we identify the Standard Model parameters with those determined by the Particle Data Group [70]. The running of the strong coupling with five active quark flavours is chosen in agreement with the selected PDF set as provided by the LHAPDF6 library [71]. As our default choice of PDFs, we employ the sets of MSHT20 [72] unless stated otherwise. To be specific, we use at LO the set MSHT20LO130 with $\alpha_s(M_Z) = 0.130$, and at NLO and NLO+NLL the set MSHT20NLO118 with and $\alpha_s(M_Z) = 0.118$. Again unless stated otherwise, we consider the dominant squark-electroweakino production channel at the LHC, *i.e.* the production of a left-handed or a right-handed up-type squark in association with the lightest neutralino.

3.1 Validation of our NLO implementation

In order to validate the numerical implementation of our NLO calculation, we compare our NLO predictions with those obtained with MADGRAPH5_AMC@NLO [73], that rely on the MSSM model implementation described in Ref. [7]. In addition, we make use of the MADSTR plugin to subtract on-shell squark and gluino contributions from the real emission pieces. We find excellent numerical agreement of the two approaches.

In addition, we validate our NLO implementation by studying the squark mass dependence of the total cross section and comparing our results to those of an independent, previously published automated calculation [6] at the MSSM benchmark point SPS1a₁₀₀₀. This benchmark is based on the point SPS1a [74], for which the physical particle spectrum is calculated with SPHENO 3 [75], and the gluino mass is then shifted to 1 TeV. Our results are presented in fig. 2. The contributions from real and virtual corrections, made individually finite with the Catani-Seymour dipole formalism [59], are also shown separately. The contributions from the integrated dipoles and the collinear counterterms $\mathbf{P} + \mathbf{K}$ have been combined with the virtual corrections. For the associated production of a right-handed

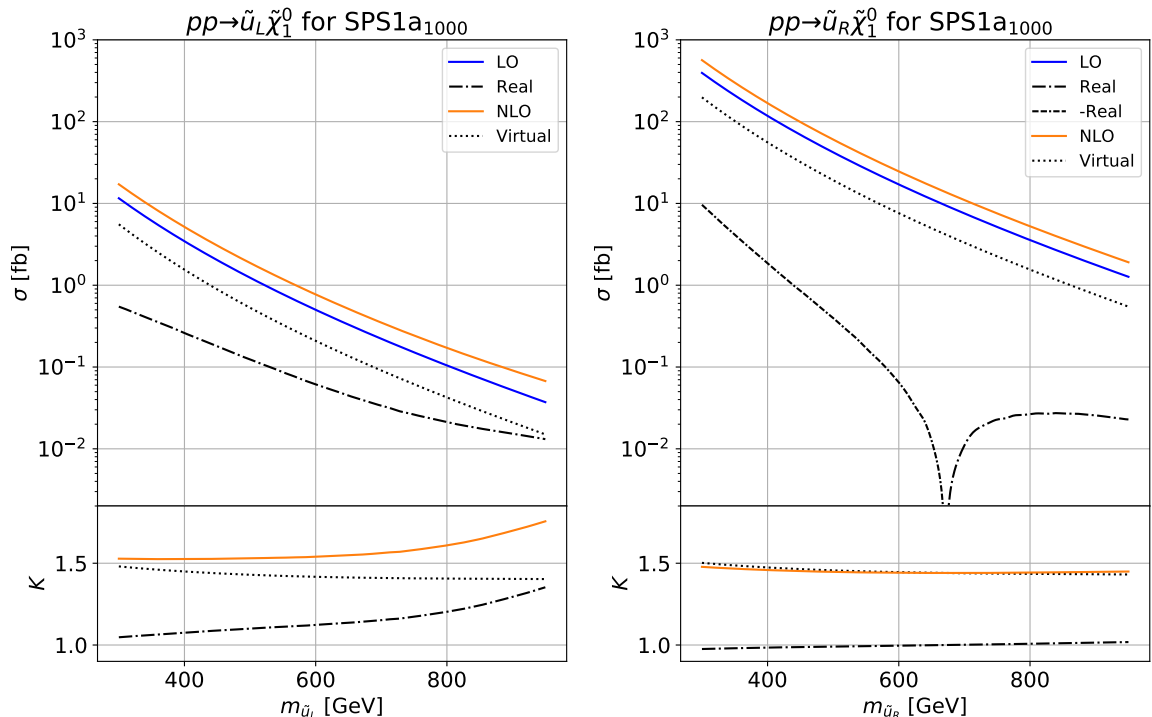


Figure 2: NLO cross sections $\sigma(pp \rightarrow \tilde{u}_{L,R}\tilde{\chi}_1^0)$ and their virtual and real components (top panels) as well as the associated K factors (bottom panels) as a function of the squark mass $m_{\tilde{u}_{L,R}}$ for a fixed mass difference $m_{\tilde{u}_L} - m_{\tilde{u}_R} = 20$ GeV. The remaining MSSM parameters are fixed to the benchmark point SPS1a₁₀₀₀, the LHC energy is $\sqrt{S} = 7$ TeV, and CTEQ6.6M PDFs are employed.

up-type squark with the lightest neutralino (right), we observe the same sign flip in the real corrections as the one that had been found in Ref. [6]. Moreover, our K -factors for the real and virtual corrections, defined by their ratios with respect to the Born cross section, exhibit the same behaviour as those in the reference computation, both for $\tilde{u}_L\tilde{\chi}_1^0$ and $\tilde{u}_R\tilde{\chi}_1^0$ production. The remaining minor numerical differences between the two calculations can be traced back to the use of a slightly different PDF set, as LHAPDF6 [71] no longer supports CTEQ6M [76], and benchmark scenario with small differences in the superpartner masses (below 1%).

Next, we demonstrate in fig. 3 that the factorisation and renormalisation scale dependence of our result agrees with the findings of Ref. [6]. In addition, we show as shaded bands the uncertainties obtained by varying the central scale $\mu_0 \equiv \mu_R = \mu_F = (m_{\tilde{q}} + m_{\tilde{\chi}})/2$ with the seven-point method, *i.e.* by varying both scales independently by a factor of two up and down, but excluding relative factors of four between the two scales. As expected, the NLO corrections increase the total cross section and reduce the scale uncertainties. For illustrative purposes, we include also our new NLL+NLO predictions (green). While they do not systematically increase the NLO cross section for the masses chosen here, the scale uncertainty is reduced by about a factor of two relative to the NLO result.

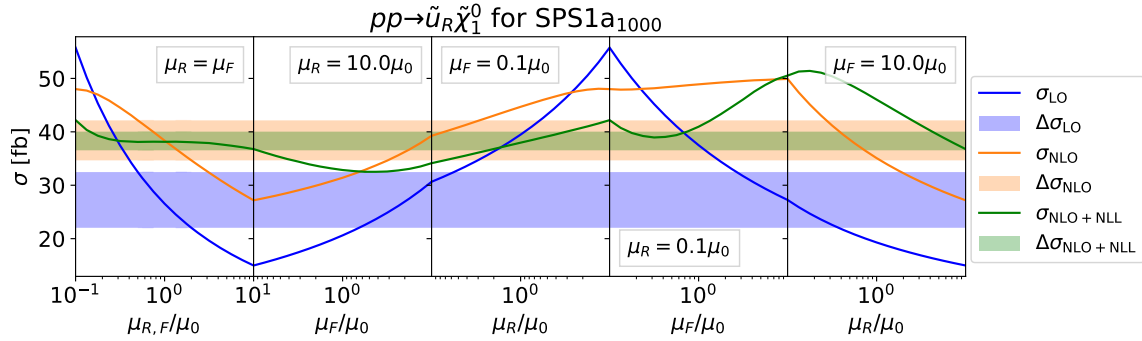


Figure 3: Profile of the renormalisation and factorisation scale dependence of the total cross section for the process $pp \rightarrow \tilde{u}_R \tilde{\chi}_1^0$. The plot covers $\mu_{F,R} \in (0.1 - 10)\mu_0$, where the central scale is $\mu_0 = (m_{\tilde{q}} + m_{\tilde{\chi}})/2$. The bands show the scale uncertainties as obtained from the seven-point method. The predictions in this plot are for a centre-of-mass energy of $\sqrt{S} = 7$ TeV and CTEQ6.6M PDFs.

pMSSM-11 scenario A			pMSSM-11 scenario B		
M_1	M_2	M_3	M_1	M_2	M_3
0.25	0.25	-3.86	0.51	0.48	3.00
$M_{(U,D,Q)_{1,2}}$	$M_{(U,D,Q)_3}$	μ	$M_{(U,D,Q)_{1,2}}$	$M_{(U,D,Q)_3}$	μ
4.0	1.7	1.33	0.9	2.0	-9.4
$M_{(L,E)_{1,2}}$	$M_{(L,E)_3}$	$\tan \beta$	$M_{(L,E)_{1,2}}$	$M_{(L,E)_3}$	$\tan \beta$
0.35	0.47	36	1.85	1.33	33
M_A	A_0		M_A	A_0	
4.0	2.8		3.0	-3.4	
$m_{\tilde{\chi}_1^0}$	$m_{\tilde{u}}$	$m_{\tilde{g}}$	$m_{\tilde{\chi}_1^0}$	$m_{\tilde{u}}$	$m_{\tilde{g}}$
0.249	4.07	3.90	0.505	0.96	2.94

Table 1: Higgs and soft SUSY breaking parameters in our pMSSM-11 benchmark models, together with the relevant resulting physical particle masses. All values, except for $\tan \beta$, are given in TeV.

3.2 Invariant mass distributions

In the following, we present results for two specific phenomenological MSSM scenarios with eleven parameters (pMSSM-11). The input parameters and the relevant resulting physical masses obtained with SPHENO 3 are listed in table 1. First, we focus on a scenario featuring large squark masses of 4 TeV, referred to as scenario A. Second, scenario B explores squark and gaugino masses expected to be within the reach of Run 3 of the LHC. Both scenarios are based on the global fits of Ref. [77]. Scenario A is derived from a fit that includes data from the anomalous magnetic moment of the muon [78], while scenario B does not include it. In addition, we have lowered the parameters M_1 and M_2 in scenario B and have increased the parameter M_3 to bring the squark and gluino masses in agreement with the

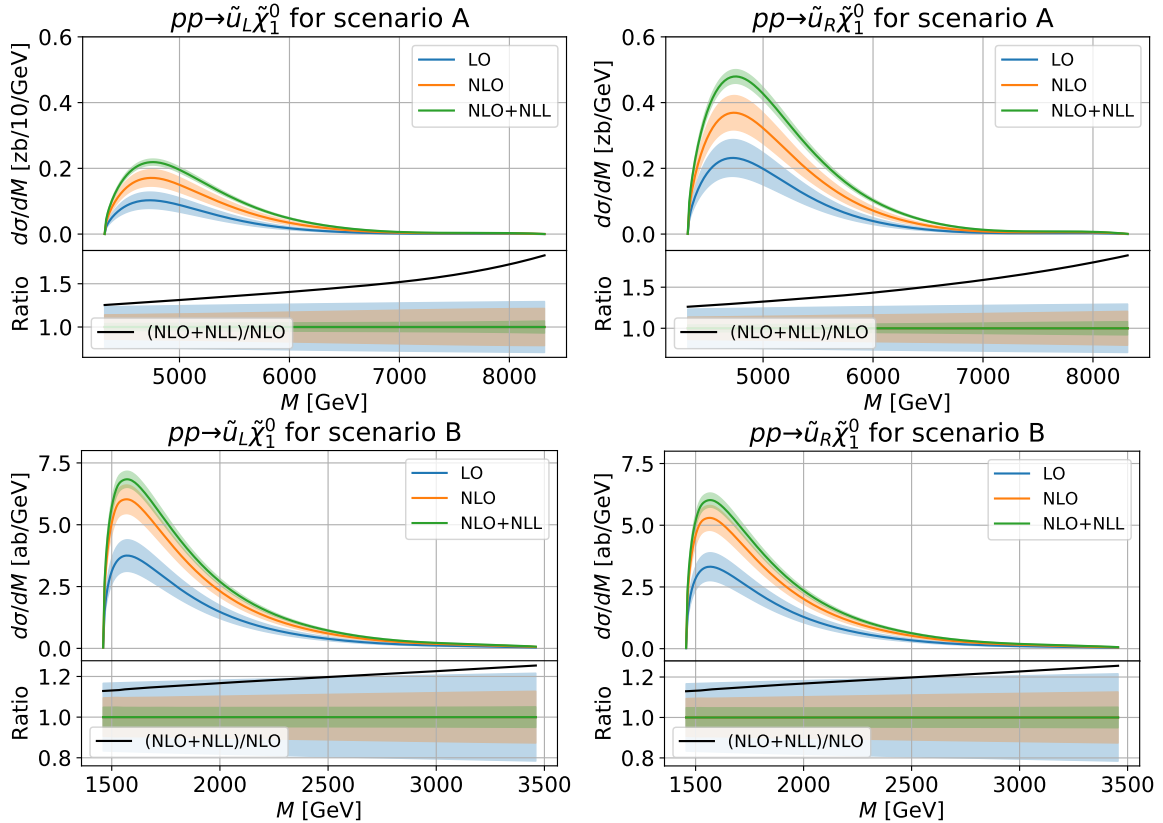


Figure 4: Invariant-mass distributions for the processes $pp \rightarrow \tilde{u}_{L,R}\tilde{\chi}_1^0$ (top panels). The uncertainties correspond to variations around the central scale $\mu_0 = M$, and we additionally show NLL+NLO/NLO K -factors (bottom panels). The results are shown for both scenarios A and B with MSHT20 PDFs and a centre-of-mass energy of $\sqrt{S} = 13$ TeV.

current SUSY limits from the LHC [40, 42, 43].

In fig. 4, we show invariant mass distributions as derived from eq. (2.34) for the associated production of left- and right-handed squarks with the lightest neutralino in both scenarios A and B. An invariant mass below the combined final state particle masses $M_0 = m_{\tilde{\chi}} + m_{\tilde{q}}$ is kinematically forbidden. Very close to this lower limit there is a rapid increase of the cross section, until it peaks at about $M \approx 1.1M_0$ and then falls off towards higher values of M . As the invariant mass M increases, we get closer to the threshold region $z = M^2/s \rightarrow 1$, and NLL corrections contribute significantly more to the differential cross section. This behaviour is captured by the NLL+NLO/NLO K -factors shown in the lower panels of the figure. For scenario A, the increase of the NLO cross section goes from 25% in the region of the peak to more than 50% at large invariant masses. In contrast, scenario B receives smaller corrections of 10% to 20% due to the smaller invariant mass M relevant for the bulk of the cross section.

The lower panels display the relative seven-point scale uncertainty, when the scale is varied around a central scale choice of $\mu_0 = M$. Across the whole mass range, the scale uncertainty is first reduced when comparing LO rates to NLO ones, and next further

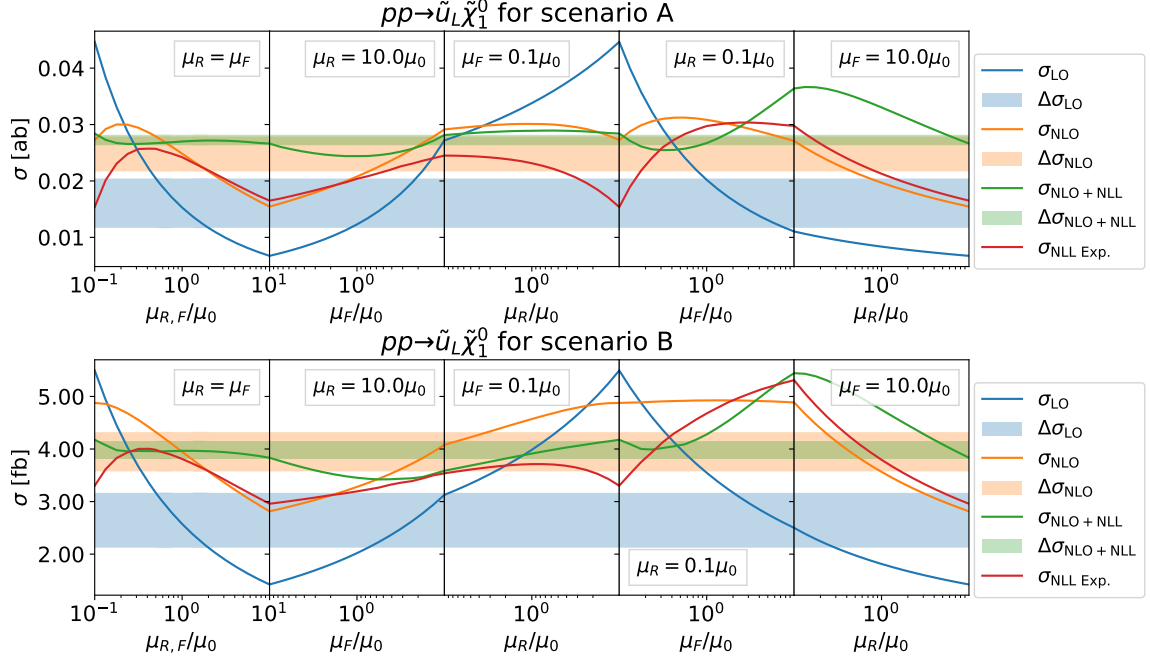


Figure 5: Profiles of the renormalisation and factorisation scale dependence of the total cross section corresponding to the process $pp \rightarrow \tilde{u}_L \tilde{\chi}_1^0$ in scenarios A and B. The plots cover $\mu \in (0.1 - 10)\mu_0$ with a central scale $\mu_0 = (m_{\tilde{q}} + m_{\tilde{\chi}})/2$. The bands correspond to scale uncertainties evaluated with the seven-point method, and we use $\sqrt{S} = 13$ TeV and MSHT20 PDFs. We present predictions at LO, NLO and NLO+NLL, as well as for the $\mathcal{O}(\alpha_s^2)$ expansion of the NLL result.

reduced when considering NLO+NLL predictions. By performing a similar calculation with $\mu_0 = (m_{\tilde{q}} + m_{\tilde{\chi}})/2$ we recover the total cross section (see below) as the area under the invariant mass distribution.

In our figures, results for the production of left-handed up-squarks in scenario A are scaled by a factor of 10. Due to the bino-like nature of the neutralino $\tilde{\chi}_1^0$ in this scenario, the coupling to the right-handed up-squark is dominant, and so is the cross section related to the production of a $\tilde{u}_R \tilde{\chi}_1^0$ pair. In scenario B however, the composition of $\tilde{\chi}_1^0$ is roughly 50% wino and 50% bino, yielding cross sections of the same order for the two processes $pp \rightarrow \tilde{u}_R \tilde{\chi}_1^0$ and $pp \rightarrow \tilde{u}_L \tilde{\chi}_1^0$.

3.3 Total cross sections and their scale uncertainty

In fig. 5, we present predictions for the total cross section related to the process $pp \rightarrow \tilde{u}_L \tilde{\chi}_1^0$ in scenarios A and B with squark masses is of 4 TeV and 1 TeV, respectively, together with the associated scale uncertainties. The results are shown at LO, NLO and NLO+NLL for a centre-of-mass energy of $\sqrt{S} = 13$ TeV. Our predictions show a significant increase of the total cross section in scenario A when including NLO+NLL corrections as well as a reduction of the scale uncertainties in both scenarios. The uncertainty bands are again determined by the seven-point method, where the factorisation and renormalisation scales are both varied

independently by factors of two up and down around the central scale $\mu_0 = (m_{\tilde{q}} + m_{\tilde{\chi}})/2$, excluding the cases where $\mu_F/\mu_R = 4$ or $1/4$. For both examined scenarios, we observe that the relative scale uncertainties are reduced from about $\pm 20\%$ at LO to $\pm 10\%$ at NLO, and finally fall below $\pm 5\%$ at NLO+NLL. The kink at $\mu_F = \mu_R = 0.1\mu_0$ is more prominent in scenario A than in scenario B. It originates from the subtraction of on-shell squark and gluino resonant contributions from the real emission component of the cross section. We also include predictions for the expansion of the NLL predictions at $\mathcal{O}(\alpha_s^2)$, following eq. (2.31) (solid red curve). As expected for large scales the logarithmic terms become dominant, and the expansion consequently approximates well the NLO result.

3.4 Parton density uncertainties of the total cross section

So far we have only studied scale uncertainties associated with the total rates for squark-electroweakino production at the LHC. There is, however, a second important source of theoretical uncertainties, *i.e.* those coming from the parton density fits. To compute them, we use the methods available in LHAPDF, which allow to calculate the PDF uncertainties in two different ways [79]:

- **Eigenvectors:** Experimental uncertainties are parametrised by making computations for a set of orthogonal Hessian PDF eigenvectors. The uncertainty is calculated from

$$\Delta\sigma_{\text{PDF}\pm} = \sqrt{\sum_{i=1}^n \left[\max(\pm\sigma_{+i} \mp \sigma_0, \pm\sigma_{-i} \mp \sigma_0, 0) \right]^2}, \quad (3.1)$$

where the index i runs over all PDF eigenvectors, with $i = 0$ representing the central, best fit, set. This method is the one to be used with CT18 [80] and MSHT20 [72] densities.

- **Replicas:** Monte Carlo PDF sets are provided with multiple replicas that need to be combined to get a statistical symmetric uncertainty on the predictions. This is achieved through the formula

$$\Delta\sigma_{\text{PDF}\pm} = \sqrt{\frac{1}{n-1} \sum_{i=1}^n \left[\sigma_i - \langle\sigma\rangle \right]^2}, \quad (3.2)$$

where the index i runs over the entire set of PDF replicas, with the central value being given by the mean cross section value $\langle\sigma\rangle = \frac{1}{n} \sum_{i=1}^n \sigma_i \simeq \sigma_0$. This method is used with NNPDF40 densities [81].

For our predictions at NLO and NLO+NLL, we calculated the PDF uncertainties at 90% confidence level. The resummation of large logarithms does not significantly alter the size of the relative PDF uncertainties, as the same set of PDFs is used in both calculations. For scenario B we show in fig. 6 the PDF uncertainties associated with NLO+NLL total cross sections for the different choices of parton densities mentioned above, *i.e.* for MSHT20, CT18 and NNPDF40. We consider the process $pp \rightarrow \tilde{u}_{L,R}\tilde{\chi}_1^0$ in the top row of the figure and

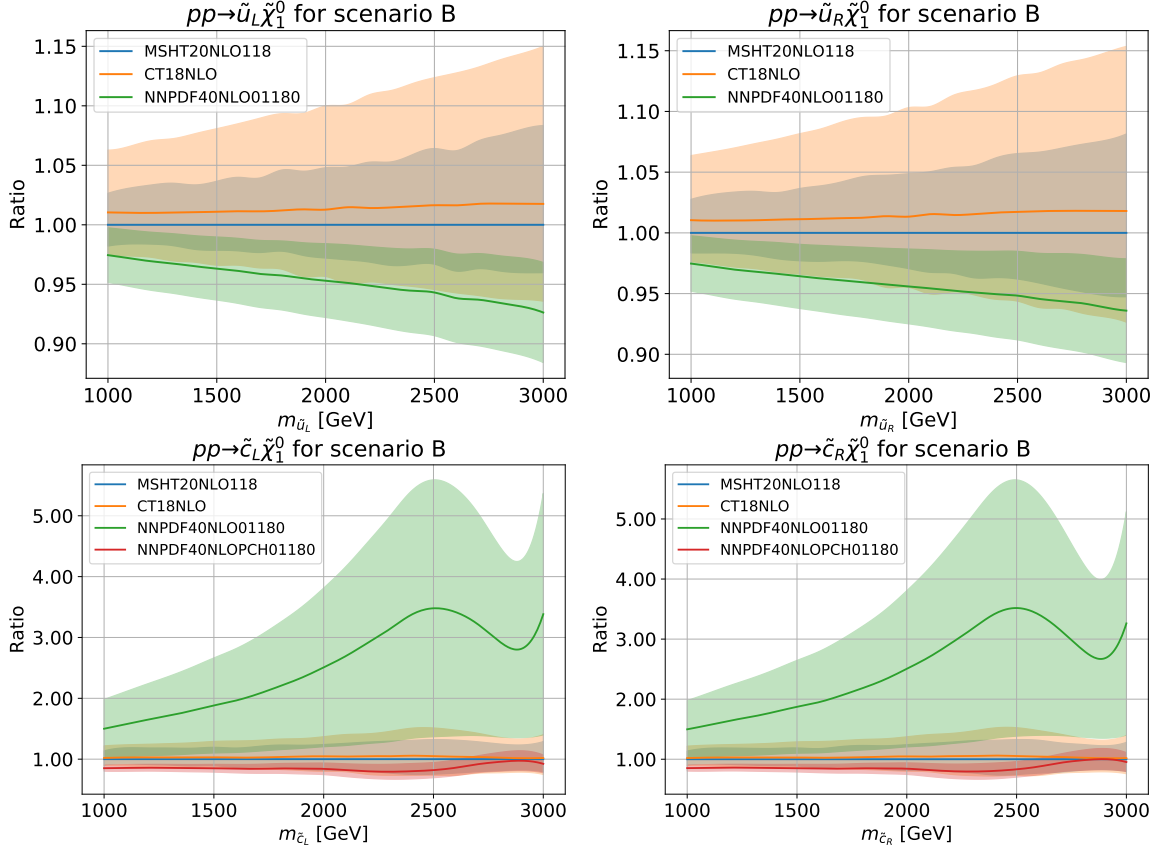


Figure 6: Relative PDF uncertainties of the total cross sections for the processes $pp \rightarrow \tilde{q}_{L,R}\tilde{\chi}_1^0$ at the LHC with a centre-of-mass energy of $\sqrt{S} = 13$ TeV and at NLO+NLL. The uncertainties are shown as a function of the squark mass $m_{\tilde{q}_{L,R}}$ and for four different choices of PDFs, namely MSHT20NLO118 (blue), CT18NLO (orange), NNPDF40NLO01180 (green) and NNPDF40NLOPCH01180 (red).

present predictions as a function of the squark mass. While the uncertainty is of about 5 % for 1 TeV up-squarks, it increases up to 10 – 15 % for squark masses of 3 TeV. This increase is related to the large partonic momentum fractions x relevant for such a large mass, where the PDFs are less constrained in their fitting procedure. The central cross section values obtained with the MSHT20 and CT18 sets agree consistently at the percent level in the explored mass range, the MSTH20 errors being slightly smaller as a consequence of this set being more recent than the CT18 one. On the other hand, the NNPDF40 predictions are a few percent lower, although they are still in reasonable agreement within their uncertainty intervals with the predictions achieved with other PDFs.

In the lower two plots of fig. 6 we show results for the production of a charm squark in association with the lightest neutralino. We observe that the results obtained with the central NNPDF40NLO01180 set with $\alpha_s(M_Z) = 0.118$ give cross sections that are larger by a factor of three to four with respect to those obtained with the CT18NLO set and with the MSHT20NLO118 set, both also with $\alpha_s(M_Z) = 0.118$. In addition, the uncertainties

associated with the NNPDF40 predictions are of about 30–50%, in contrast with predictions obtained with CT18 and MSHT20, that have much smaller uncertainties. This discrepancy can be traced back to the treatment of the charm quark in the NNPDF40 fit [82] and is expected to be even more significant in processes with two charm quarks or antiquarks in the initial state. The cross sections estimated with the alternative NNPDF40NLOPCH01180 PDF fit (red) with $\alpha_s(M_Z) = 0.118$, in which the treatment of the charm quark is kept purely perturbative, are, in contrast, in good agreement with CT18 and MSHT20 both for the central values and the uncertainties.

3.5 Squark and gaugino mass dependence of the total cross section

The dependence of the total cross section for associated squark-electroweakino production on the masses of the produced particles is important to estimate the sensitivity of Run 3 at the LHC to this process. A precise quantitative statement would of course require a detailed signal and background analysis, which is beyond the scope of this work. Therefore, we show in Fig. 7 the total cross sections and resulting relative scale uncertainties for scenario B as a function of the SUSY particle masses, both for $\tilde{u}_L\tilde{\chi}_1^0$ (left) and $\tilde{u}_R\tilde{\chi}_1^0$ (right) production. As expected, the cross sections fall steeply with either mass. Our predictions indicate that an integrated luminosity of 350 fb^{-1} at $\sqrt{S} = 13\text{ TeV}$ from the LHC Run 3 [3] will lead to the production of hundreds of squark-electroweakino events for a neutralino mass of 0.5 TeV and squark masses ranging up to 2 TeV.

In the lower panels of the plots, we observe an improvement in the precision of the predictions over the whole mass range. Resummation effects reduce the scale dependence from $\pm 10\%$ at NLO to below $\pm 5\%$ at NLO+NLL. The black curves in the lower insets of the figures represent the ratio of the NLO+NLL predictions to the NLO ones and demonstrate the increasing impact of resummation with rising mass values. As in the previous sections, this demonstrates once more that resummation effects are larger near the hadronic threshold. While the central cross section values are enlarged by 50% when adding NLO corrections to the LO rates, the additional increase from NLL resummation reaches only about 6% for the mass ranges observable at the LHC in the near future.

4 Conclusion

We have presented in this paper a threshold resummation calculation at the NLO+NLL accuracy for the associated production of a squark and an electroweakino at the LHC. This process has the potential to become important in the near future, if squarks and gluinos turn out to be too heavy to be produced in pairs. The semi-strong production of one electroweak and one strongly-interacting superpartner indeed offers cross sections of intermediate size and a larger available phase space thanks to the possibility of having a lighter electroweakino in the final state.

Our investigations required the calculation of the full NLO corrections to the LO rate, as well as of the associated process-dependent soft anomalous dimension and hard matching coefficients. By matching fixed-order and resummed predictions, we consistently combined the resummation of large logarithms appearing close to threshold at NLL with NLO results.

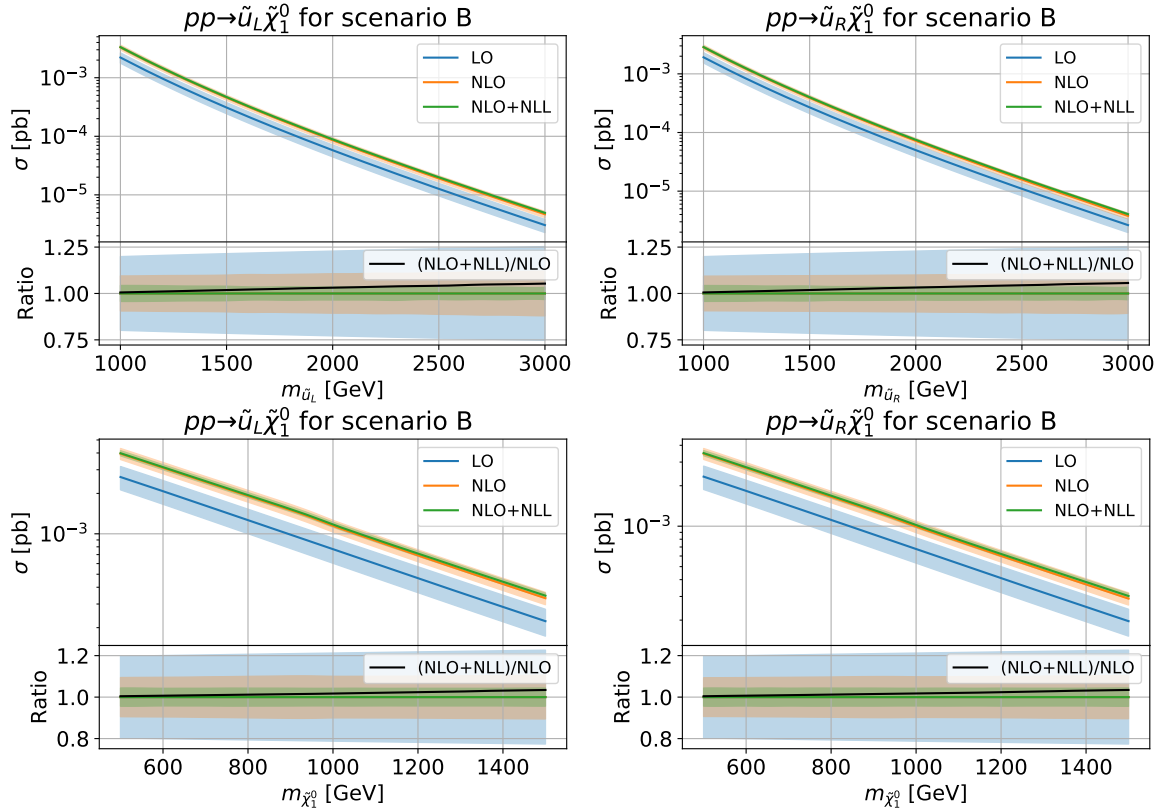


Figure 7: Total cross sections for the processes $pp \rightarrow \tilde{u}_{L,R} \tilde{\chi}_1^0$ and their relative scale uncertainties (top panels) as well as (NLO+NLL)/NLO K -factors (bottom panels) in scenario B. In the first row, we vary the squark mass $m_{\tilde{u}_{L,R}}$, keeping a fixed distance between the left- and right-handed squark masses $m_{\tilde{u}_L} - m_{\tilde{u}_R} = 100$ GeV. In the second row, we vary the electroweakino mass $m_{\tilde{\chi}}$. The other parameters defining scenario B are not modified. The LHC energy is $\sqrt{S} = 13$ TeV, and we use MSHT20 PDFs.

NLL resummation has been found to increase the NLO cross sections by up to 6% for squark masses expected to be in the reach of the LHC Run 3. In addition, the resummation procedure allowed for a stabilisation of the predictions relative to the scale dependence, the scale uncertainties being reduced to below 5% in the explored mass regime. Our calculation will be included in the next version of the public code RESUMMINO [83].

Acknowledgments

We thank M. Sunder for his collaboration in the early stages of this project. This work has been supported by the BMBF under contract 05P21PMCAA and by the DFG through the Research Training Network 2149 “Strong and Weak Interactions - from Hadrons to Dark Matter”.

Open Access. This article is distributed under the terms of the Creative Commons Attribution License (CC-BY-4.0), which permits any use, distribution and reproduction in

any medium, provided the original author(s) and source are credited.

A Soft anomalous dimension

We compute the soft anomalous dimension $\bar{\Gamma}$ for squark-electroweakino production

$$\bar{\Gamma}_{ab \rightarrow ij} = \Gamma_{ab \rightarrow ij} - \Gamma_{ab}^{\text{DY}} \quad (\text{A.1})$$

with

$$\Gamma_{ab \rightarrow ij} = - \sum_{kl} C^{kl} \lim_{\epsilon \rightarrow 0} \epsilon \omega^{kl}. \quad (\text{A.2})$$

In this expression, the sum goes over eikonal lines, C^{kl} are colour factors, which depend on each specific diagram, ω^{kl} are integrals over the corresponding kinematic quantities and Γ^{DY} includes the contribution from the self-energies of the two incoming Wilson lines. The latter is given by

$$\Gamma_{ab}^{\text{DY}} = \frac{\alpha_s}{2\pi} \sum_{k=\{a,b\}} C_k \left[1 - \log \left(\frac{(v_k \cdot n)^2}{|n|^2} \right) - \log(2) - i\pi \right] \delta_{IJ}, \quad (\text{A.3})$$

where the sum goes over the initial-state particles and the colour factor C_k is equal to C_F for an incoming (anti)quark and to C_A for an incoming gluon. The four-momentum n^μ is an axial gauge vector fulfilling $|n|^2 = -n^2 - i\epsilon$ [12]. The factor δ_{IJ} indicates that this contribution has to be subtracted from the diagonal elements in the colour basis of the process. In the process considered in this work, the soft anomalous dimension is a scalar quantity, since we are dealing with a colour basis containing a single element due to the presence of a single coloured final-state particle.

We can write a general expression for the integrals ω^{kl}

$$\omega^{kl} = g_s \int \frac{d^D q}{(2\pi)^D} \frac{-i}{q^2 + i\epsilon} \left[\frac{\Delta_k \Delta_l v_k \cdot v_l}{(\delta_k v_k \cdot q + i\epsilon)(\delta_l v_l \cdot q + i\epsilon)} - \frac{\delta_l \Delta_l \Delta_k v_k \cdot n}{\delta_k v_k \cdot q + i\epsilon} \frac{P}{(n \cdot q)} - \frac{\delta_k \Delta_k \Delta_l v_l \cdot n}{\delta_l v_l \cdot q + i\epsilon} \frac{P}{(n \cdot q)} + n^2 \delta_k \Delta_k \delta_l \Delta_l \frac{P}{(n \cdot q)^2} \right], \quad (\text{A.4})$$

where we used the eikonal Feynman rules found in Ref. [84]. The above integral depends on the principal value operator P , that is calculated as

$$\frac{P}{(n \cdot q)^\beta} = \frac{1}{2} \left(\frac{1}{(n \cdot q + i\epsilon)^\beta} + (-1)^\beta \frac{1}{(-n \cdot q + i\epsilon)^\beta} \right), \quad (\text{A.5})$$

on $v_i^\mu = p_i^\mu \sqrt{2/s}$, and on the process-dependent signs Δ and δ .

We use the solutions of Ref. [85] for the integrals associated with the diagrams in fig. 8. We obtain similar expressions as in Ref. [29], apart from the combined signs $S_{kl} = \Delta_k \Delta_l \delta_k \delta_l$

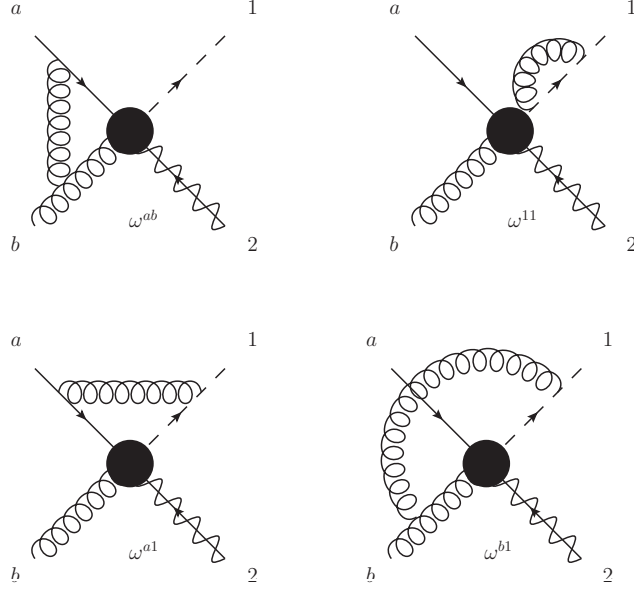


Figure 8: Eikonal diagrams for the soft anomalous dimension in squark-electroweakino production.

that are given by $S_{ab} = -1$, $S_{a1} = +1$, $S_{b1} = +1$ and $S_{11} = -1$. To be specific, we obtain

$$\omega^{ab} = S_{ab} \frac{\alpha_s}{\epsilon\pi} \left[-\log\left(\frac{v_a \cdot v_b}{2}\right) + \frac{1}{2} \log\left(\frac{(v_a \cdot n)^2 (v_b \cdot n)^2}{|n|^2 |n|^2}\right) + i\pi - 1 \right], \quad (\text{A.6})$$

$$\omega^{a1} = S_{a1} \frac{\alpha_s}{\epsilon\pi} \left[-\frac{1}{2} \log\left(\frac{(v_a \cdot v_1)^2 s}{2m_q^2}\right) + L_1 + \frac{1}{2} \log\left(\frac{(v_a \cdot n)^2}{|n|^2}\right) - 1 \right], \quad (\text{A.7})$$

$$\omega^{b1} = S_{b1} \frac{\alpha_s}{\epsilon\pi} \left[-\frac{1}{2} \log\left(\frac{(v_b \cdot v_1)^2 s}{2m_q^2}\right) + L_1 + \frac{1}{2} \log\left(\frac{(v_b \cdot n)^2}{|n|^2}\right) - 1 \right], \quad (\text{A.8})$$

$$\omega^{11} = S_{11} \frac{\alpha_s}{\epsilon\pi} [2L_1 - 2]. \quad (\text{A.9})$$

For squark-electroweakino production, the final-state massive particle is a squark, so that the kinematic quantities read

$$v_a \cdot v_b = \frac{2p_a \cdot p_b}{s} = 1, \quad v_a \cdot v_1 = \frac{2p_a \cdot p_1}{s} = \frac{m_q^2 - t}{s} \quad \text{and} \quad v_b \cdot v_1 = \frac{2p_b \cdot p_1}{s} = \frac{m_q^2 - u}{s}, \quad (\text{A.10})$$

where t and u are the usual Mandelstam variables. The remaining quantity L_1 simplifies to one in the limit $(v_1 \cdot n)^2 \rightarrow 2m_q^2 n^2/s$.

The relevant colour factors C^{kl} are

$$\begin{aligned} C^{ab} &= \frac{\text{Tr}[\mathbf{T}^i \mathbf{T}^{i'} \mathbf{T}^j] (-i) f^{i'ij}}{\text{Tr}[\mathbf{T}^i \mathbf{T}^i]} = -\frac{C_A}{2}, & C^{11} &= \frac{\text{Tr}[\mathbf{T}^i \mathbf{T}^j \mathbf{T}^j \mathbf{T}^i]}{\text{Tr}[\mathbf{T}^i \mathbf{T}^i]} = C_F, \\ C^{a1} &= \frac{\text{Tr}[\mathbf{T}^i \mathbf{T}^j \mathbf{T}^i \mathbf{T}^j]}{\text{Tr}[\mathbf{T}^i \mathbf{T}^i]} = C_F - \frac{C_A}{2}, & C^{b1} &= \frac{\text{Tr}[\mathbf{T}^i \mathbf{T}^j \mathbf{T}^{i'}] (-i) f^{i'ij}}{\text{Tr}[\mathbf{T}^i \mathbf{T}^i]} = \frac{C_A}{2}, \end{aligned} \quad (\text{A.11})$$

where we have used the well-known relation $T^a T^a = C_F \mathbf{1}$.

With these ingredients we can calculate $\Gamma_{ab \rightarrow ij}$

$$\Gamma_{ab \rightarrow ij} = \epsilon \left[-C_F(\omega^{a1} + \omega^{11}) + \frac{C_A}{2}(\omega^{ab} + \omega^{a1} - \omega^{b1}) \right] \quad (\text{A.12})$$

$$\begin{aligned} &= \frac{\alpha_s}{2\pi} \left[C_F \left(-\log \left(\frac{(v_a \cdot n)^2}{|n|^2} \right) + \log \left(\frac{(v_a \cdot v_1)^2 s}{2m_{\tilde{q}}^2} \right) + 2L_1 - 2 \right) \right. \\ &\quad \left. + C_A \left(-\frac{1}{2} \log \left(\frac{(v_a \cdot v_1)^2 s}{2m_{\tilde{q}}^2} \right) + \frac{1}{2} \log \left(\frac{(v_b \cdot v_1)^2 s}{2m_{\tilde{q}}^2} \right) \right. \right. \\ &\quad \left. \left. - \log \left(\frac{(v_b \cdot n)^2}{|n|^2} \right) + \log \left(\frac{v_a \cdot v_b}{2} \right) + 1 - i\pi \right) \right], \quad (\text{A.13}) \end{aligned}$$

while the contribution from the initial-state self energies is

$$\begin{aligned} \Gamma_{ab}^{\text{DY}} &= \frac{\alpha_s}{2\pi} \left[C_F \left(1 - \log \left(\frac{(v_a \cdot n)^2}{|n|^2} \right) - \log(2) - i\pi \right) \right. \\ &\quad \left. + C_A \left(1 - \log \left(\frac{(v_b \cdot n)^2}{|n|^2} \right) - \log(2) - i\pi \right) \right]. \quad (\text{A.14}) \end{aligned}$$

We observe the cancellation of the gauge dependent terms. This gives as the final result for the soft anomalous dimension

$$\begin{aligned} \bar{\Gamma}_{ab \rightarrow ij} &= \frac{\alpha_s}{2\pi} \left\{ C_F \left[\log \left(\frac{(v_a \cdot v_1)^2 s}{2m_{\tilde{q}}^2} \right) + 2L_1 - 3 + \log(2) + i\pi \right] + \right. \\ &\quad \left. + C_A \left[-\frac{1}{2} \log \left(\frac{(v_a \cdot v_1)^2 s}{2m_{\tilde{q}}^2} \right) + \frac{1}{2} \log \left(\frac{(v_b \cdot v_1)^2 s}{2m_{\tilde{q}}^2} \right) + \log \left(\frac{v_a \cdot v_b}{2} \right) + \log(2) \right] \right\} \\ &= \frac{\alpha_s}{2\pi} \left\{ C_F \left[2 \log \left(\frac{m_{\tilde{q}}^2 - t}{\sqrt{s} m_{\tilde{q}}} \right) - 1 + i\pi \right] + C_A \log \left(\frac{m_{\tilde{q}}^2 - u}{m_{\tilde{q}}^2 - t} \right) \right\}. \quad (\text{A.15}) \end{aligned}$$

B Lists of total cross sections

In table 2 and table 3, we show the total cross sections for the associated production of an up-type squark and the lightest neutralino at NLO and NLO+NLL accuracy for an LHC centre-of-mass energy of $\sqrt{S} = 13$ TeV in scenario B. The results are listed both as a function of the squark mass and of the neutralino mass and correspond to the plots in fig. 7. We give the scale and PDF uncertainty for the resummed result for the three PDFs we already investigated in fig. 6, namely MSHT20NLO118, CT18NLO and NNPDF40.

References

- [1] H. P. Nilles, *Supersymmetry, Supergravity and Particle Physics*, *Phys. Rept.* **110** (1984) 1–162.
- [2] H. E. Haber and G. L. Kane, *The Search for Supersymmetry: Probing Physics Beyond the Standard Model*, *Phys. Rept.* **117** (1985) 75–263.

$m_{\tilde{u}_L}$ [GeV]	NLO ^{+scale+PDF} _{-scale-PDF} [fb]	NLO+NLL ^{+scale+PDF} _{-scale-PDF} [fb]		
	MSHT20NLO118	MSHT20NLO118	CT18NLO	NNPDF40
1000	3.301 ^{+9.5%+2.4%} _{-9.5%-2.0%}	3.318 ^{+4.7%+2.6%} _{-3.9%-1.8%}	3.353 ^{+4.7%+5.2%} _{-3.9%-3.4%}	3.234 ^{+4.7%+2.4%} _{-3.9%-2.4%}
1100	2.148 ^{+9.6%+2.7%} _{-9.5%-2.1%}	2.166 ^{+4.5%+3.1%} _{-3.8%-1.6%}	2.188 ^{+4.6%+5.5%} _{-3.8%-3.6%}	2.105 ^{+4.6%+2.4%} _{-3.8%-2.4%}
1200	1.426 ^{+9.6%+2.8%} _{-9.6%-2.1%}	1.442 ^{+4.4%+3.3%} _{-3.8%-1.6%}	1.456 ^{+4.5%+6.0%} _{-3.7%-3.7%}	1.398 ^{+4.5%+2.5%} _{-3.7%-2.5%}
1300	0.963 ^{+9.7%+3.0%} _{-9.7%-2.3%}	0.976 ^{+4.3%+3.5%} _{-3.7%-1.7%}	0.986 ^{+4.3%+6.1%} _{-3.7%-4.0%}	0.944 ^{+4.4%+2.6%} _{-3.7%-2.6%}
1400	0.660 ^{+9.7%+3.1%} _{-9.9%-2.4%}	0.671 ^{+4.2%+3.4%} _{-3.7%-2.1%}	0.678 ^{+4.3%+6.5%} _{-3.6%-4.2%}	0.647 ^{+4.4%+2.7%} _{-3.6%-2.7%}
1500	0.458 ^{+9.8%+3.4%} _{-10.0%-2.5%}	0.467 ^{+4.2%+3.7%} _{-3.6%-2.1%}	0.472 ^{+4.2%+6.9%} _{-3.6%-4.4%}	0.450 ^{+4.3%+2.7%} _{-3.6%-2.7%}
1600	0.322 ^{+9.9%+3.6%} _{-10.1%-2.6%}	0.329 ^{+4.1%+4.0%} _{-3.5%-2.2%}	0.332 ^{+4.1%+7.3%} _{-3.5%-4.5%}	0.316 ^{+4.2%+2.8%} _{-3.5%-2.8%}
1700	0.229 ^{+10.0%+3.6%} _{-10.2%-2.9%}	0.234 ^{+4.0%+3.9%} _{-3.5%-2.3%}	0.237 ^{+4.1%+7.7%} _{-3.5%-4.7%}	0.224 ^{+4.2%+2.9%} _{-3.4%-2.9%}
1800	0.164 ^{+10.2%+4.2%} _{-10.4%-2.7%}	0.168 ^{+4.0%+4.6%} _{-3.5%-2.2%}	0.170 ^{+4.0%+8.0%} _{-3.4%-4.9%}	0.161 ^{+4.1%+3.0%} _{-3.4%-3.0%}
1900	0.118 ^{+10.2%+4.1%} _{-10.5%-3.2%}	0.122 ^{+3.9%+4.5%} _{-3.5%-2.6%}	0.123 ^{+3.9%+8.0%} _{-3.4%-5.6%}	0.116 ^{+4.1%+3.1%} _{-3.4%-3.1%}
2000	0.086 ^{+10.4%+4.4%} _{-10.6%-3.4%}	0.089 ^{+3.9%+4.8%} _{-3.4%-2.8%}	0.090 ^{+3.9%+8.6%} _{-3.3%-5.5%}	0.084 ^{+4.0%+3.2%} _{-3.3%-3.2%}
2100	0.063 ^{+10.5%+4.7%} _{-10.7%-3.3%}	0.065 ^{+3.8%+4.9%} _{-3.4%-2.9%}	0.066 ^{+3.8%+8.5%} _{-3.4%-6.3%}	0.062 ^{+4.0%+3.4%} _{-3.3%-3.4%}
2200	0.046 ^{+10.7%+5.2%} _{-10.9%-3.4%}	0.048 ^{+3.8%+5.3%} _{-3.3%-3.1%}	0.049 ^{+3.8%+9.4%} _{-3.3%-6.1%}	0.046 ^{+4.0%+3.5%} _{-3.2%-3.5%}
2300	0.034 ^{+10.9%+5.3%} _{-11.1%-3.7%}	0.036 ^{+3.7%+5.3%} _{-3.3%-3.4%}	0.036 ^{+3.8%+9.7%} _{-3.3%-6.4%}	0.034 ^{+3.9%+3.6%} _{-3.2%-3.6%}
2400	0.026 ^{+10.9%+5.8%} _{-11.2%-3.7%}	0.027 ^{+3.7%+5.9%} _{-3.2%-3.3%}	0.027 ^{+3.7%+10.2%} _{-3.3%-6.6%}	0.025 ^{+3.8%+3.7%} _{-3.2%-3.7%}
2500	0.019 ^{+11.2%+6.3%} _{-11.3%-3.6%}	0.020 ^{+3.7%+6.4%} _{-3.2%-3.3%}	0.020 ^{+3.6%+10.5%} _{-3.3%-7.0%}	0.019 ^{+3.7%+3.8%} _{-3.3%-3.8%}
2600	0.014 ^{+11.3%+6.3%} _{-11.4%-4.1%}	0.015 ^{+3.5%+6.2%} _{-3.3%-3.9%}	0.015 ^{+3.6%+10.9%} _{-3.3%-7.2%}	0.014 ^{+3.8%+4.0%} _{-3.1%-4.0%}
2700	0.011 ^{+11.5%+7.1%} _{-11.6%-3.9%}	0.011 ^{+3.5%+7.0%} _{-3.2%-3.7%}	0.011 ^{+3.5%+11.3%} _{-3.2%-7.6%}	0.011 ^{+3.7%+4.1%} _{-3.1%-4.1%}
2800	0.008 ^{+11.7%+7.6%} _{-11.7%-4.1%}	0.009 ^{+3.5%+7.5%} _{-3.2%-3.9%}	0.009 ^{+3.4%+11.9%} _{-3.2%-7.8%}	0.008 ^{+3.6%+4.2%} _{-3.2%-4.2%}
2900	0.006 ^{+11.9%+8.2%} _{-11.8%-4.1%}	0.006 ^{+3.4%+8.0%} _{-3.1%-4.0%}	0.007 ^{+3.3%+12.4%} _{-3.2%-7.9%}	0.006 ^{+3.5%+4.4%} _{-3.2%-4.4%}
3000	0.005 ^{+11.8%+8.5%} _{-11.9%-4.2%}	0.005 ^{+3.4%+8.3%} _{-3.0%-4.0%}	0.005 ^{+3.3%+13.0%} _{-3.2%-8.0%}	0.005 ^{+3.5%+4.5%} _{-3.1%-4.5%}

Table 2: Total cross sections for $pp \rightarrow \tilde{u}_L \tilde{\chi}_1^0$ at $\sqrt{S} = 13$ TeV at NLO and NLO+NLL for various squark masses, with a fixed mass difference between left- and right-handed squarks of $m_{\tilde{u}_L} - m_{\tilde{u}_R} = 100$ GeV, and PDFs. The remaining parameters are fixed to scenario B.

$m_{\tilde{\chi}_1^0}$ [GeV]	NLO ^{+scale+PDF} _{-scale-PDF} [fb]	NLO+NLL ^{+scale+PDF} _{-scale-PDF} [fb]		
	MSHT20NLO118	MSHT20NLO118	CT18NLO	NNPDF40
500	3.950 ^{+9.5%+2.3%} _{-9.4%-2.3%}	3.966 ^{+4.7%+2.4%} _{-3.9%-2.1%}	4.007 ^{+4.8%+4.8%} _{-3.9%-3.6%}	3.867 ^{+4.8%+2.3%} _{-3.9%-2.3%}
550	3.502 ^{+9.6%+2.4%} _{-9.5%-2.2%}	3.521 ^{+4.7%+2.6%} _{-3.8%-2.0%}	3.556 ^{+4.8%+5.0%} _{-3.8%-3.6%}	3.429 ^{+4.8%+2.4%} _{-3.8%-2.4%}
600	3.102 ^{+9.6%+2.4%} _{-9.6%-2.2%}	3.123 ^{+4.7%+2.5%} _{-3.8%-2.0%}	3.154 ^{+4.8%+5.1%} _{-3.8%-3.6%}	3.039 ^{+4.8%+2.4%} _{-3.8%-2.4%}
650	2.748 ^{+9.7%+2.6%} _{-9.6%-2.1%}	2.769 ^{+4.7%+2.7%} _{-3.8%-2.0%}	2.797 ^{+4.7%+5.4%} _{-3.8%-3.7%}	2.692 ^{+4.8%+2.5%} _{-3.8%-2.5%}
700	2.434 ^{+9.8%+2.7%} _{-9.7%-2.1%}	2.456 ^{+4.7%+2.9%} _{-3.8%-1.9%}	2.481 ^{+4.7%+5.5%} _{-3.8%-3.8%}	2.385 ^{+4.8%+2.5%} _{-3.8%-2.5%}
750	2.158 ^{+9.9%+2.7%} _{-9.8%-2.2%}	2.180 ^{+4.6%+2.8%} _{-3.9%-2.0%}	2.202 ^{+4.7%+5.6%} _{-3.8%-3.8%}	2.115 ^{+4.7%+2.5%} _{-3.9%-2.5%}
800	1.913 ^{+10.1%+2.6%} _{-9.9%-2.4%}	1.936 ^{+4.6%+2.8%} _{-3.9%-2.2%}	1.955 ^{+4.6%+5.9%} _{-3.9%-3.8%}	1.876 ^{+4.6%+2.5%} _{-3.9%-2.5%}
850	1.697 ^{+10.2%+3.0%} _{-10.0%-2.1%}	1.718 ^{+4.5%+3.1%} _{-3.9%-1.9%}	1.736 ^{+4.6%+6.2%} _{-3.9%-3.6%}	1.664 ^{+4.6%+2.6%} _{-3.9%-2.6%}
900	1.502 ^{+10.3%+3.0%} _{-10.1%-2.2%}	1.523 ^{+4.5%+3.0%} _{-3.9%-2.0%}	1.538 ^{+4.5%+6.4%} _{-3.9%-3.8%}	1.473 ^{+4.6%+2.6%} _{-3.9%-2.6%}
950	1.319 ^{+10.3%+3.3%} _{-10.1%-2.1%}	1.340 ^{+4.6%+3.4%} _{-3.8%-1.9%}	1.353 ^{+4.6%+6.6%} _{-3.8%-3.8%}	1.295 ^{+4.6%+2.7%} _{-3.8%-2.7%}
1000	1.146 ^{+10.0%+3.2%} _{-10.0%-2.4%}	1.166 ^{+4.7%+3.3%} _{-3.7%-2.2%}	1.178 ^{+4.8%+6.8%} _{-3.7%-4.0%}	1.125 ^{+4.8%+2.7%} _{-3.7%-2.7%}
1050	1.007 ^{+10.0%+3.4%} _{-10.0%-2.4%}	1.025 ^{+4.9%+3.7%} _{-3.6%-2.0%}	1.036 ^{+4.9%+7.2%} _{-3.6%-3.9%}	0.988 ^{+5.0%+2.8%} _{-3.6%-2.8%}
1100	0.887 ^{+10.0%+3.6%} _{-10.1%-2.4%}	0.904 ^{+4.9%+4.0%} _{-3.5%-1.9%}	0.914 ^{+5.0%+7.7%} _{-3.5%-4.0%}	0.870 ^{+5.1%+2.8%} _{-3.5%-2.8%}
1150	0.782 ^{+10.0%+3.8%} _{-10.1%-2.4%}	0.799 ^{+5.0%+4.1%} _{-3.5%-2.0%}	0.808 ^{+5.1%+7.9%} _{-3.5%-4.0%}	0.768 ^{+5.2%+2.9%} _{-3.5%-2.9%}
1200	0.691 ^{+10.0%+4.0%} _{-10.2%-2.5%}	0.706 ^{+5.1%+4.3%} _{-3.5%-2.0%}	0.715 ^{+5.2%+8.2%} _{-3.5%-4.2%}	0.679 ^{+5.2%+2.9%} _{-3.5%-2.9%}
1250	0.610 ^{+10.1%+4.1%} _{-10.2%-2.5%}	0.625 ^{+5.2%+4.6%} _{-3.5%-1.8%}	0.633 ^{+5.2%+8.3%} _{-3.5%-4.3%}	0.600 ^{+5.3%+2.9%} _{-3.5%-2.9%}
1300	0.540 ^{+10.1%+4.3%} _{-10.3%-2.5%}	0.554 ^{+5.3%+5.2%} _{-3.5%-1.4%}	0.560 ^{+5.3%+8.4%} _{-3.5%-4.6%}	0.531 ^{+5.4%+3.0%} _{-3.5%-3.0%}
1350	0.478 ^{+10.2%+4.0%} _{-10.3%-3.1%}	0.491 ^{+5.4%+4.9%} _{-3.5%-2.1%}	0.497 ^{+5.4%+8.4%} _{-3.6%-4.9%}	0.470 ^{+5.5%+3.0%} _{-3.6%-3.0%}
1400	0.423 ^{+10.3%+4.1%} _{-10.4%-3.2%}	0.435 ^{+5.4%+5.2%} _{-3.6%-2.0%}	0.440 ^{+5.5%+8.4%} _{-3.6%-5.3%}	0.416 ^{+5.6%+3.1%} _{-3.7%-3.1%}
1450	0.374 ^{+10.3%+4.2%} _{-10.5%-3.3%}	0.386 ^{+5.5%+5.3%} _{-3.6%-2.1%}	0.391 ^{+5.5%+8.3%} _{-3.7%-5.6%}	0.369 ^{+5.6%+3.1%} _{-3.7%-3.1%}
1500	0.332 ^{+10.4%+4.3%} _{-10.6%-3.5%}	0.342 ^{+5.6%+5.5%} _{-3.7%-2.2%}	0.347 ^{+5.6%+8.7%} _{-3.7%-5.6%}	0.327 ^{+5.7%+3.2%} _{-3.8%-3.2%}

Table 3: Total cross sections for $pp \rightarrow \tilde{u}_L \tilde{\chi}_1^0$ at $\sqrt{S} = 13$ TeV at NLO and NLO+NLL for various neutralino masses and PDFs. The remaining parameters are fixed to scenario B.

- [3] I. Zurbano Fernandez et al., *High-Luminosity Large Hadron Collider (HL-LHC): Technical design report*, CERN-2020-010.
- [4] X. Cid Vidal et al., *Report from Working Group 3: Beyond the Standard Model physics at the HL-LHC and HE-LHC*, *CERN Yellow Rep. Monogr.* **7** (2019) 585–865, [[arXiv:1812.07831](#)].
- [5] F. Gianotti et al., *Physics potential and experimental challenges of the LHC luminosity upgrade*, *Eur. Phys. J. C* **39** (2005) 293–333, [[hep-ph/0204087](#)].
- [6] T. Binoth, D. Goncalves Netto, D. Lopez-Val, K. Mawatari, T. Plehn, and I. Wigmore, *Automized Squark-Neutralino Production to Next-to-Leading Order*, *Phys. Rev. D* **84** (2011) 075005, [[arXiv:1108.1250](#)].
- [7] S. Frixione, B. Fuks, V. Hirschi, K. Mawatari, H.-S. Shao, P. A. Sunder, and M. Zaro, *Automated simulations beyond the Standard Model: supersymmetry*, *JHEP* **12** (2019) 008, [[arXiv:1907.04898](#)].
- [8] J. Baglio, G. Coniglio, B. Jager, and M. Spira, *Next-to-leading-order QCD corrections and parton-shower effects for weakino+squark production at the LHC*, *JHEP* **12** (2021) 020, [[arXiv:2110.04211](#)].
- [9] G. F. Sterman, *Summation of Large Corrections to Short Distance Hadronic Cross-Sections*, *Nucl. Phys. B* **281** (1987) 310–364.
- [10] S. Catani and L. Trentadue, *Resummation of the QCD Perturbative Series for Hard Processes*, *Nucl. Phys. B* **327** (1989) 323–352.
- [11] S. Catani and L. Trentadue, *Comment on QCD exponentiation at large x* , *Nucl. Phys. B* **353** (1991) 183–186.
- [12] N. Kidonakis and G. F. Sterman, *Resummation for QCD hard scattering*, *Nucl. Phys. B* **505** (1997) 321–348, [[hep-ph/9705234](#)].
- [13] N. Kidonakis, G. Oderda, and G. F. Sterman, *Threshold resummation for dijet cross-sections*, *Nucl. Phys. B* **525** (1998) 299–332, [[hep-ph/9801268](#)].
- [14] G. Bozzi, B. Fuks, and M. Klasen, *Slepton production in polarized hadron collisions*, *Phys. Lett. B* **609** (2005) 339–350, [[hep-ph/0411318](#)].
- [15] G. Bozzi, B. Fuks, and M. Klasen, *Transverse-momentum resummation for slepton-pair production at the CERN LHC*, *Phys. Rev. D* **74** (2006) 015001, [[hep-ph/0603074](#)].
- [16] G. Bozzi, B. Fuks, and M. Klasen, *Threshold Resummation for Slepton-Pair Production at Hadron Colliders*, *Nucl. Phys. B* **777** (2007) 157–181, [[hep-ph/0701202](#)].
- [17] G. Bozzi, B. Fuks, and M. Klasen, *Joint resummation for slepton pair production at hadron colliders*, *Nucl. Phys. B* **794** (2008) 46–60, [[arXiv:0709.3057](#)].
- [18] B. Fuks, M. Klasen, D. R. Lamprea, and M. Rothering, *Revisiting slepton pair production at the Large Hadron Collider*, *JHEP* **01** (2014) 168, [[arXiv:1310.2621](#)].
- [19] J. Fiaschi and M. Klasen, *Slepton pair production at the LHC in NLO+NLL with resummation-improved parton densities*, *JHEP* **03** (2018) 094, [[arXiv:1801.10357](#)].
- [20] J. Fiaschi, M. Klasen, and M. Sunder, *Slepton pair production with aNNLO+NNLL precision*, *JHEP* **04** (2020) 049, [[arXiv:1911.02419](#)].
- [21] J. Debove, B. Fuks, and M. Klasen, *Model-independent analysis of gaugino-pair production in polarized and unpolarized hadron collisions*, *Phys. Rev. D* **78** (2008) 074020, [[arXiv:0804.0423](#)].

- [22] J. Debove, B. Fuks, and M. Klasen, *Transverse-momentum resummation for gaugino-pair production at hadron colliders*, *Phys. Lett. B* **688** (2010) 208–211, [[arXiv:0907.1105](#)].
- [23] J. Debove, B. Fuks, and M. Klasen, *Threshold resummation for gaugino pair production at hadron colliders*, *Nucl. Phys. B* **842** (2011) 51–85, [[arXiv:1005.2909](#)].
- [24] J. Debove, B. Fuks, and M. Klasen, *Joint Resummation for Gaugino Pair Production at Hadron Colliders*, *Nucl. Phys. B* **849** (2011) 64–79, [[arXiv:1102.4422](#)].
- [25] B. Fuks, M. Klasen, D. R. Lamprea, and M. Rothering, *Gaugino production in proton-proton collisions at a center-of-mass energy of 8 TeV*, *JHEP* **10** (2012) 081, [[arXiv:1207.2159](#)].
- [26] B. Fuks, M. Klasen, D. R. Lamprea, and M. Rothering, *Precision predictions for electroweak superpartner production at hadron colliders with Resummino*, *Eur. Phys. J. C* **73** (2013) 2480, [[arXiv:1304.0790](#)].
- [27] J. Fiaschi and M. Klasen, *Neutralino-chargino pair production at NLO+NLL with resummation-improved parton density functions for LHC Run II*, *Phys. Rev. D* **98** (2018), no. 5 055014, [[arXiv:1805.11322](#)].
- [28] J. Fiaschi and M. Klasen, *Higgsino and gaugino pair production at the LHC with aNNLO+NNLL precision*, *Phys. Rev. D* **102** (2020), no. 9 095021, [[arXiv:2006.02294](#)].
- [29] B. Fuks, M. Klasen, and M. Rothering, *Soft gluon resummation for associated gluino-gaugino production at the LHC*, *JHEP* **07** (2016) 053, [[arXiv:1604.01023](#)].
- [30] A. Kulesza and L. Motyka, *Threshold resummation for squark-antisquark and gluino-pair production at the LHC*, *Phys. Rev. Lett.* **102** (2009) 111802, [[arXiv:0807.2405](#)].
- [31] W. Beenakker, S. Brensing, M. Kramer, A. Kulesza, E. Laenen, and I. Niessen, *NNLL resummation for squark-antisquark pair production at the LHC*, *JHEP* **01** (2012) 076, [[arXiv:1110.2446](#)].
- [32] W. Beenakker, C. Borschensky, R. Heger, M. Krämer, A. Kulesza, and E. Laenen, *NNLL resummation for stop pair-production at the LHC*, *JHEP* **05** (2016) 153, [[arXiv:1601.02954](#)].
- [33] W. Beenakker, S. Brensing, M. Kramer, A. Kulesza, E. Laenen, and I. Niessen, *Soft-gluon resummation for squark and gluino hadroproduction*, *JHEP* **12** (2009) 041, [[arXiv:0909.4418](#)].
- [34] W. Beenakker, T. Janssen, S. Lepoeter, M. Krämer, A. Kulesza, E. Laenen, I. Niessen, S. Thewes, and T. Van Daal, *Towards NNLL resummation: hard matching coefficients for squark and gluino hadroproduction*, *JHEP* **10** (2013) 120, [[arXiv:1304.6354](#)].
- [35] W. Beenakker, C. Borschensky, M. Krämer, A. Kulesza, E. Laenen, V. Theeuwes, and S. Thewes, *NNLL resummation for squark and gluino production at the LHC*, *JHEP* **12** (2014) 023, [[arXiv:1404.3134](#)].
- [36] W. Beenakker, C. Borschensky, M. Krämer, A. Kulesza, E. Laenen, S. Marzani, and J. Rojo, *NLO+NLL squark and gluino production cross-sections with threshold-improved parton distributions*, *Eur. Phys. J. C* **76** (2016), no. 2 53, [[arXiv:1510.00375](#)].
- [37] J. L. Feng, S. Su, and F. Takayama, *Lower limit on dark matter production at the large hadron collider*, *Phys. Rev. Lett.* **96** (2006) 151802, [[hep-ph/0503117](#)].
- [38] Y. Bai, P. J. Fox, and R. Harnik, *The Tevatron at the Frontier of Dark Matter Direct Detection*, *JHEP* **12** (2010) 048, [[arXiv:1005.3797](#)].

- [39] CMS Collaboration, A. M. Sirunyan et al., *Search for supersymmetry in multijet events with missing transverse momentum in proton-proton collisions at 13 TeV*, *Phys. Rev. D* **96** (2017), no. 3 032003, [[arXiv:1704.07781](#)].
- [40] CMS Collaboration, A. M. Sirunyan et al., *Search for supersymmetry in proton-proton collisions at 13 TeV in final states with jets and missing transverse momentum*, *JHEP* **10** (2019) 244, [[arXiv:1908.04722](#)].
- [41] CMS Collaboration, A. Tumasyan et al., *Search for electroweak production of charginos and neutralinos in proton-proton collisions at $\sqrt{s} = 13$ TeV*, [arXiv:2106.14246](#).
- [42] ATLAS Collaboration, G. Aad et al., *Search for squarks and gluinos in final states with jets and missing transverse momentum using 139 fb⁻¹ of $\sqrt{s} = 13$ TeV pp collision data with the ATLAS detector*, *JHEP* **02** (2021) 143, [[arXiv:2010.14293](#)].
- [43] ATLAS Collaboration, G. Aad et al., *Search for squarks and gluinos in final states with one isolated lepton, jets, and missing transverse momentum at $\sqrt{s} = 13$ with the ATLAS detector*, *Eur. Phys. J. C* **81** (2021), no. 7 600, [[arXiv:2101.01629](#)]. [Erratum: *Eur.Phys.J.C* **81**, 956 (2021)].
- [44] J. C. Collins, D. E. Soper, and G. F. Sterman, *Factorization of Hard Processes in QCD*, *Adv. Ser. Direct. High Energy Phys.* **5** (1989) 1–91, [[hep-ph/0409313](#)].
- [45] J. F. Gunion and H. E. Haber, *Higgs Bosons in Supersymmetric Models. 1.*, *Nucl. Phys. B* **272** (1986) 1. [Erratum: *Nucl.Phys.B* **402**, 567–569 (1993)].
- [46] G. Bozzi, B. Fuks, and M. Klasen, *Non-diagonal and mixed squark production at hadron colliders*, *Phys. Rev. D* **72** (2005) 035016, [[hep-ph/0507073](#)].
- [47] G. Bozzi, B. Fuks, B. Herrmann, and M. Klasen, *Squark and gaugino hadroproduction and decays in non-minimal flavour violating supersymmetry*, *Nucl. Phys. B* **787** (2007) 1–54, [[arXiv:0704.1826](#)].
- [48] B. Fuks, B. Herrmann, and M. Klasen, *Flavour Violation in Gauge-Mediated Supersymmetry Breaking Models: Experimental Constraints and Phenomenology at the LHC*, *Nucl. Phys. B* **810** (2009) 266–299, [[arXiv:0808.1104](#)].
- [49] B. Fuks, B. Herrmann, and M. Klasen, *Phenomenology of anomaly-mediated supersymmetry breaking scenarios with non-minimal flavour violation*, *Phys. Rev. D* **86** (2012) 015002, [[arXiv:1112.4838](#)].
- [50] K. De Causmaecker, B. Fuks, B. Herrmann, F. Mahmoudi, B. O’Leary, W. Porod, S. Sekmen, and N. Strobbe, *General squark flavour mixing: constraints, phenomenology and benchmarks*, *JHEP* **11** (2015) 125, [[arXiv:1509.05414](#)].
- [51] A. Chakraborty, M. Endo, B. Fuks, B. Herrmann, M. M. Nojiri, P. Pani, and G. Polesello, *Flavour-violating decays of mixed top-charm squarks at the LHC*, *Eur. Phys. J. C* **78** (2018), no. 10 844, [[arXiv:1808.07488](#)].
- [52] R. Gavin, C. Hangst, M. Krämer, M. Mühlleitner, M. Pellen, E. Popena, and M. Spira, *Matching Squark Pair Production at NLO with Parton Showers*, *JHEP* **10** (2013) 187, [[arXiv:1305.4061](#)].
- [53] W. Hollik, J. M. Lindert, and D. Pagani, *NLO corrections to squark-squark production and decay at the LHC*, *JHEP* **03** (2013) 139, [[arXiv:1207.1071](#)].
- [54] J. C. Collins, F. Wilczek, and A. Zee, *Low-Energy Manifestations of Heavy Particles: Application to the Neutral Current*, *Phys. Rev. D* **18** (1978) 242.

- [55] W. A. Bardeen, A. J. Buras, D. W. Duke, and T. Muta, *Deep Inelastic Scattering Beyond the Leading Order in Asymptotically Free Gauge Theories*, *Phys. Rev. D* **18** (1978) 3998.
- [56] W. J. Marciano, *Flavor Thresholds and Lambda in the Modified Minimal Subtraction Prescription*, *Phys. Rev. D* **29** (1984) 580.
- [57] S. P. Martin and M. T. Vaughn, *Regularization dependence of running couplings in softly broken supersymmetry*, *Phys. Lett. B* **318** (1993) 331–337, [[hep-ph/9308222](#)].
- [58] S. Catani and M. H. Seymour, *A General algorithm for calculating jet cross-sections in NLO QCD*, *Nucl. Phys. B* **485** (1997) 291–419, [[hep-ph/9605323](#)]. [Erratum: *Nucl.Phys.B* 510, 503–504 (1998)].
- [59] S. Catani, S. Dittmaier, M. H. Seymour, and Z. Trocsanyi, *The Dipole formalism for next-to-leading order QCD calculations with massive partons*, *Nucl. Phys. B* **627** (2002) 189–265, [[hep-ph/0201036](#)].
- [60] S. Catani, S. Dittmaier, and Z. Trocsanyi, *One loop singular behavior of QCD and SUSY QCD amplitudes with massive partons*, *Phys. Lett. B* **500** (2001) 149–160, [[hep-ph/0011222](#)].
- [61] T. Kinoshita, *Mass singularities of Feynman amplitudes*, *J. Math. Phys.* **3** (1962) 650–677.
- [62] T. D. Lee and M. Nauenberg, *Degenerate Systems and Mass Singularities*, *Phys. Rev.* **133** (1964) B1549–B1562.
- [63] A. Vogt, *Next-to-next-to-leading logarithmic threshold resummation for deep inelastic scattering and the Drell-Yan process*, *Phys. Lett. B* **497** (2001) 228–234, [[hep-ph/0010146](#)].
- [64] M. Kramer, E. Laenen, and M. Spira, *Soft gluon radiation in Higgs boson production at the LHC*, *Nucl. Phys. B* **511** (1998) 523–549, [[hep-ph/9611272](#)].
- [65] S. Catani, D. de Florian, and M. Grazzini, *Higgs production in hadron collisions: Soft and virtual QCD corrections at NNLO*, *JHEP* **05** (2001) 025, [[hep-ph/0102227](#)].
- [66] A. Kulesza, G. F. Sterman, and W. Vogelsang, *Joint resummation in electroweak boson production*, *Phys. Rev. D* **66** (2002) 014011, [[hep-ph/0202251](#)].
- [67] L. G. Almeida, G. F. Sterman, and W. Vogelsang, *Threshold Resummation for Di-hadron Production in Hadronic Collisions*, *Phys. Rev. D* **80** (2009) 074016, [[arXiv:0907.1234](#)].
- [68] S. Catani, M. L. Mangano, P. Nason, and L. Trentadue, *The Resummation of soft gluons in hadronic collisions*, *Nucl. Phys. B* **478** (1996) 273–310, [[hep-ph/9604351](#)].
- [69] H. Contopanagos and G. F. Sterman, *Principal value resummation*, *Nucl. Phys. B* **419** (1994) 77–104, [[hep-ph/9310313](#)].
- [70] **Particle Data Group** Collaboration, P. A. Zyla et al., *Review of Particle Physics*, *PTEP* **2020** (2020), no. 8 083C01.
- [71] A. Buckley, J. Ferrando, S. Lloyd, K. Nordström, B. Page, M. Rüfenacht, M. Schönherr, and G. Watt, *LHAPDF6: parton density access in the LHC precision era*, *Eur. Phys. J. C* **75** (2015) 132, [[arXiv:1412.7420](#)].
- [72] S. Bailey, T. Cridge, L. A. Harland-Lang, A. D. Martin, and R. S. Thorne, *Parton distributions from LHC, HERA, Tevatron and fixed target data: MSHT20 PDFs*, *Eur. Phys. J. C* **81** (2021), no. 4 341, [[arXiv:2012.04684](#)].
- [73] J. Alwall, R. Frederix, S. Frixione, V. Hirschi, F. Maltoni, O. Mattelaer, H. S. Shao, T. Stelzer, P. Torrielli, and M. Zaro, *The automated computation of tree-level and*

next-to-leading order differential cross sections, and their matching to parton shower simulations, *JHEP* **07** (2014) 079, [[arXiv:1405.0301](https://arxiv.org/abs/1405.0301)].

- [74] B. C. Allanach et al., *The Snowmass Points and Slopes: Benchmarks for SUSY Searches*, *Eur. Phys. J. C* **25** (2002) 113–123, [[hep-ph/0202233](https://arxiv.org/abs/hep-ph/0202233)].
- [75] W. Porod and F. Staub, *SPheno 3.1: Extensions including flavour, CP-phases and models beyond the MSSM*, *Comput. Phys. Commun.* **183** (2012) 2458–2469, [[arXiv:1104.1573](https://arxiv.org/abs/1104.1573)].
- [76] J. Pumplin, D. R. Stump, J. Huston, H. L. Lai, P. M. Nadolsky, and W. K. Tung, *New generation of parton distributions with uncertainties from global QCD analysis*, *JHEP* **07** (2002) 012, [[hep-ph/0201195](https://arxiv.org/abs/hep-ph/0201195)].
- [77] E. Bagnaschi et al., *Likelihood Analysis of the pMSSM11 in Light of LHC 13-TeV Data*, *Eur. Phys. J. C* **78** (2018), no. 3 256, [[arXiv:1710.11091](https://arxiv.org/abs/1710.11091)].
- [78] **Muon g-2** Collaboration, B. Abi et al., *Measurement of the Positive Muon Anomalous Magnetic Moment to 0.46 ppm*, *Phys. Rev. Lett.* **126** (2021), no. 14 141801, [[arXiv:2104.03281](https://arxiv.org/abs/2104.03281)].
- [79] J. Butterworth et al., *PDF4LHC recommendations for LHC Run II*, *J. Phys. G* **43** (2016) 023001, [[arXiv:1510.03865](https://arxiv.org/abs/1510.03865)].
- [80] T.-J. Hou et al., *New CTEQ global analysis of quantum chromodynamics with high-precision data from the LHC*, *Phys. Rev. D* **103** (2021), no. 1 014013, [[arXiv:1912.10053](https://arxiv.org/abs/1912.10053)].
- [81] R. D. Ball et al., *The Path to Proton Structure at One-Percent Accuracy*, [arXiv:2109.02653](https://arxiv.org/abs/2109.02653).
- [82] J. Rojo, *Progress in the NNPDF global analyses of proton structure*, in *55th Rencontres de Moriond on QCD and High Energy Interactions*, 4, 2021. [arXiv:2104.09174](https://arxiv.org/abs/2104.09174).
- [83] “Resummino.” <https://resummino.hepforge.org/>.
- [84] M. Rothering, *Precise predictions for supersymmetric particle production at the LHC*. dissertation, Westfälischen Wilhelms-Universität Münster, 2016.
- [85] V. M. Theeuwes, *Soft Gluon Resummation for Heavy Particle Production at the Large Hadron Collider*. dissertation, Westfälischen Wilhelms-Universität Münster, 2015.